SEMARAK ILMU PUBLISHING

Journal of Advanced Research in Fluid Mechanics and Thermal Sciences

Journal homepage:
https://semarakilmu.com.my/journals/index.php/fluid_mechanics_thermal_sciences/index
ISSN: 2289-7879

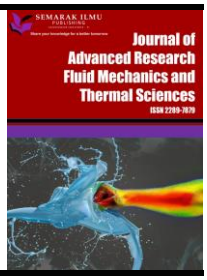


# Thermal Radiation Effect on Mixed Convective Casson Fluid Flow over a Porous Stretching Sheet with Variable Fluid Properties

Neelufer Z. Basha[1], F. Mebarek-Oudina[2], Rajashekhar Choudhari[3], Hanumesh Vaidya[1], Balachandra Hadimani[4,*], K. V. Prasad[3], Manjunatha Gudekote[4], Sangeeta Kalal[1]

[1] Department of Mathematics, Vijayanagara Sri Krishnadevaraya University, Ballari, India
[2] Department of Physics, Faculty of Sciences, University of 20 Aout 1955-Skikda, B. P. 26, 21000 Skikda, Algeria
[3] Department of Mathematics, Manipal Institute of Technology Bengaluru, Manipal Academy of Higher Education, Manipal, India
[4] Department of Mathematics, Manipal Institute of Technology, Manipal Academy of Higher Education, Manipal, India

**ARTICLE INFO**

***Article history:***
Received 25 July 2023
Received in revised form 13 October 2023
Accepted 25 October 2023
Available online 15 November 2023

***Keywords:***
Casson fluid; material parameters; variable viscosity; thermal and species diffusion

**ABSTRACT**

The effects of the variation of radiation and fluid characteristics on the flow, heat transfer, and mass transfer of a non-Newtonian Casson fluid at a vertical permeable stretched sheet are explored. We focus on the assumption that the behavior of the particles in the fluid is sensitive to both temperature and species diffusion, and we investigate their combined impacts. By using an appropriate similarity transformation, the governing nonlinear partial differential equations are converted into a system of highly nonlinear coupled ordinary differential equations. We apply a semi-analytical method for different physical parameters to solve the resultant system with proper boundary conditions. By employing the optimal homotopy analysis method (OHAM), which allows for the regulation and modification of the convergence zone, we are able to derive analytical solutions for the dimensionless velocity, temperature, and concentration fields. Our findings demonstrate that, compared to the homotopy analysis approach (HAM) proposed by Liao [1], OHAM solutions are more accurate approximations of the precise solutions for large values of the independent variable. By plotting the residual errors and comparing them to results in the literature, we can ensure that our analytical solution is correct for certain edge situations. Our method was validated by the comparison, which showed a high degree of agreement. Due to the presence of permeability parameter the velocity profile decreases, whereas the temperature and concentration profile increases. Since radiation parameter is directly connected to the free stream temperature, increasing values of radiation parameter, the thermal boundary layer thickness gets enhanced.

## 1. Introduction

Many engineering and industrial procedures rely heavily on permeability flows. These movements occur in porous mediums like filtration systems, oil storage tanks, and subterranean water reservoirs. Geothermal energy extraction, oil recovery, and heat exchangers are just a few of

* *Corresponding author.*
*E-mail address: bs.hadimani@manipal.edu*

https://doi.org/10.37934/arfmts.111.1.127

the many technical sectors that may benefit from understanding mixed convective permeable flows. Many industrial processes, including filtration, separation, and catalytic reactions, have important implications for species transport in such flows, so they have been the subject of extensive research. Adding in other physical phenomena like heat and mass transport complicates the interpretation of the already complex behavior of fluid flow in porous media. In addition, fluid qualities like viscosity and density can vary widely across a wide range of temperatures and concentrations. As a result, research into the dynamics of mixed convective permeable flows with thermo- and species-diffusion variables necessitates the creation of precise mathematical models.

In view of the above, many scientists have studied how fluids move through porous media. The concept of porous media is applied in many areas of applied science and engineering: filtration, mechanics, acoustics, geomechanics, soil mechanics, rock mechanics, petroleum engineering, bioremediation, construction engineering, geosciences, etc. Heat transmission was shown to be very sensitive to both porosity and the Prandtl number. Many other researchers examined the flow through porous medium [2-10]. Multiple studies have investigated the impact of radiation on permeable flows. They discovered that raising the radiation parameter improved the temperature and velocity distributions [11-17].

Heat and mass transfer with chemical reaction analysis is essential for chemical industries due to its numerous applications in several branches of science and engineering, such as in drying, evaporation, reservoir engineering, manufacturing of ceramics, and food processing. The order of chemical reaction depends on various factors such as foreign mass, active fluid, and stretching of the sheet, among others. Chambré and Young [18] studied the first-order chemical reaction and analyzed the diffusion of a chemically reactive species in a laminar boundary-layer flow. Muthucumaraswamy [19] considered the homogeneous chemical reaction of the first order and presented the heat and mass transfer effects on a vertical isothermal surface with uniform suction. Chamkha [20] extended the work of Muthucumaraswamy [19] to heat generation/absorption in the presence of a magnetic field. Sohail *et al.,* [21] examined the second-order slip flow and convective heat transfer of a nanofluid over a porous vertical plate with chemical reaction effects. Recently, Basha *et al.,* [22] examined the impacts of a nonlinearly expanding sheet on velocity, heat and mass transport for a Suttery hybrid nanoliquid [23-28].

All of the above studies have restricted their analyses to heat transfer over a horizontal or vertical plate, with or without chemical reaction, and assumed the thermo-physical properties of the ambient fluid to be constant. However, the two important physical properties, fluid viscosity and fluid thermal conductivity, may change with temperature [29-31].

Although many studies have been done on permeable flows, the mixed convective permeable flow of a Casson fluid with varying fluid properties, thermal and species diffusion, and radiation effects is poorly understood. To address this knowledge gap, the present work investigates Casson fluid's mixed convective permeable flow in a porous medium under the combined impacts of radiation, changeable fluid characteristics, temperature, and species diffusion. There have been several attempts to study mixed convective and permeable flows using various numerical approaches. The use of finite element, finite volume, and finite difference techniques has become commonplace. Recent years have seen the rise of computational fluid dynamics (CFD) as an effective method for investigating fluid flow in porous media. Computational fluid dynamics (CFD) allows for the simulation of intricate geometries and fluid flow phenomena and offers precise data on flow properties, including velocity, pressure, and temperature.

In this work, we examine the impact of radiation on the mixed convective permeable flow of Casson fluid with thermal and species diffusion as independent variables. Non-Newtonian fluids with a yield stress, such as paints, drilling fluids, and blood, are often described using the Casson fluid

model. Radiation, fluid variability, and species diffusion are all considered in depth as they affect the flow. This research will hopefully shed light on how fluid characteristics, temperature, and species diffusion interact in mixed convective and permeable flows. This research aims to understand better the dynamics of Casson fluid mixed convective permeable flow in a porous medium with varying fluid characteristics, thermal and species diffusion, and radiation. Research into mixed convective and permeable flows will likely yield useful information for engineering process design and optimization. Casson fluid in a porous medium undergoing convective flow, heat and species diffusion, and fluid property variability.

## 2. Problem Formulation

Consider a steady, two-dimensional mixed convective boundary layer flow of a viscous incompressible, non-Newtonian Casson fluid with variable fluid properties in porous medium with permeability $K_p^*$ and in the presence of a transverse magnetic field. The rheological equation of state for an isotropic and incompressible Casson fluid is given by [32-35]

$$\tau_{ij} = \begin{cases} 2\left(\mu_B + P_y / \sqrt{2\pi}\right)e_{ij}, \pi > \pi_c \\ 2\left(\mu_B + p_y / \sqrt{2\pi_c}\right)e_{ij}, \pi < \pi_c \end{cases} \tag{1}$$

where $\pi = e_{ij}e_{ij}$ and $e_{ij}$ is the $(i, j)^{th}$ component of deformation rate, $\pi$ is the product of the component of deformation rate with itself, $\pi_c$ is a critical value of this product based on the non-Newtonian model, $\mu_B$ is the plastic dynamic viscosity of non-Newtonian fluid, and $P_y$ is the yield stress of the fluid.

The origin is fixed at O (see Figure 1). Two equal and opposite forces are applied along the *x*-axis to stretch the porous sheet, keeping the origin fixed. The coordinate system has its origin located at the centre of the sheet with the *x*-axis extending along the sheet, while the y-axis is measured normal to the surface of the sheet and is positive in the direction from the sheet to the fluid. The flow is due to the combined buoyancy effects of temperature and concentration gradients. The sheet is drawn continuously with a nonlinear (power-law) velocity variations $U_w(x)$, the prescribed surface temperature variation $T_w(x)$ and the prescribed species diffusion variations $C_w(x)$ in the following forms [36]

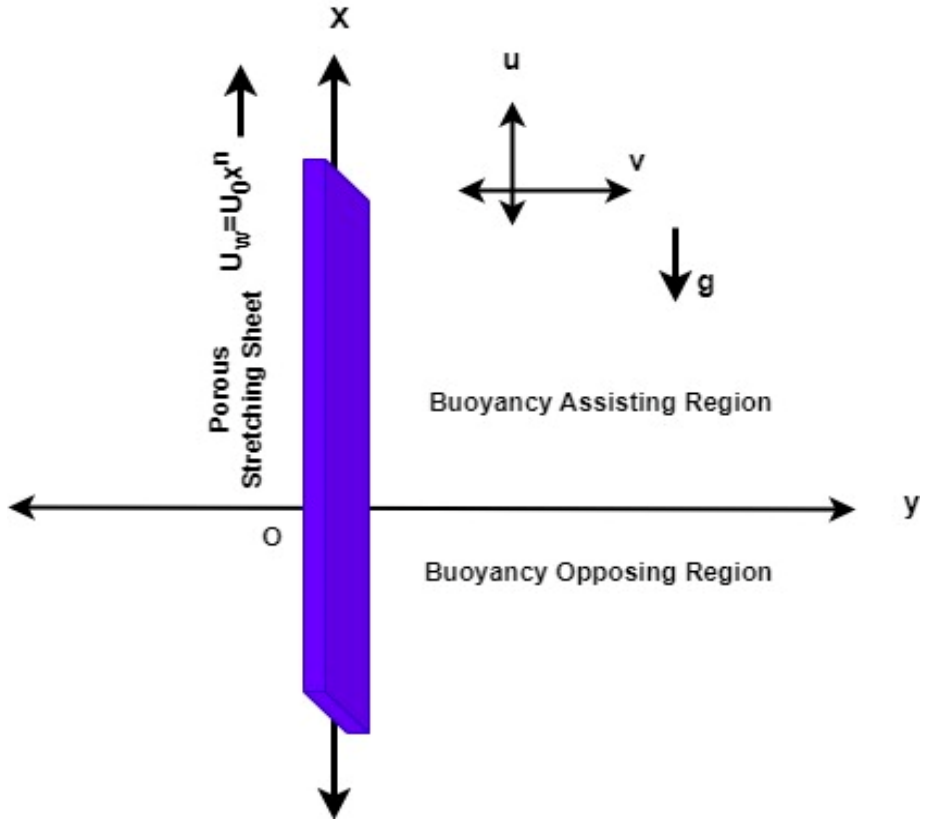


**Fig. 1.** Schematic diagram of the physical problem and coordinate system

$$U_w(x) = U_0 x^n,$$
$$T_w(x) = T_\infty + Ax^r,$$
$$C_w(x) = C_\infty + Bx^s$$

where $U_0$ the speed of the stretching sheet and $n$ the velocity exponent parameter. Positive and negative values of $n$ indicates the acceleration and deceleration of the sheet respectively. The parameters $A \text{and} B$ are the positive constants; $r \text{and} s$ are the exponents; $T_\infty$ and $C_\infty$ are the temperature and concentration fields of the fluid far away from the sheet respectively. A magnetic field of strength $B_0(x)$ is applied along the direction normal to the stretching sheet. Further, following assumptions were considered:

(i) The Magnetic Reynolds number is assumed to be small.
(ii) The electric field due to the polarization of charges is negligible.

Under these assumptions and invoking the Boussinesq approximation, the governing equations for the convective flow of Casson fluid can be written as [37]

$$u_x + \mathrm{v}_y = 0, \tag{2}$$

$$uu_x + \mathrm{v}\mathrm{u}_y = \rho_\infty^{-1}\left(1+\beta^{-1}\right)\left(\mu \mathrm{u}_y\right)_y \pm g\beta_T\left(T-T_\infty\right) + g\beta_C\left(C-C_\infty\right) - \mu\left(\rho K_p^*\right)^{-1} u, \tag{3}$$

$$uT_x + \mathrm{vT_y} = \left(\rho_\infty C_p\right)^{-1}\left(kT_y\right)_y + Q(x)\left(\rho_\infty C_p\right)^{-1}(T - T_\infty) - \left((\rho_\infty Cp)_f\right)^{-1} q_y, \tag{4}$$

$$uC_x + \mathrm{vC_y} = \left(D(C)\mathrm{C_y}\right)_y - K_m(x)\left(C - C_\infty\right)^m, \tag{5}$$

where $u$ and $\mathrm{v}$ are the velocity components in the $x$ and $y$ directions respectively, $\rho_\infty$ is the density of the fluid, $g$ is the gravitational acceleration, $\beta_T$ and $\beta_C$ are the thermal and concentration expansion coefficient respectively. $T$ is the temperature of the fluid , $C$ is the concentration of the fluid, $\sigma$ is the fluid electrical conductivity, $B_0(x)$ is the magnetic field, $C_p$ is the specific heat at constant pressure, $Q(x)$ represents respectively. The exothermic $Q > 0$ represents the heat generation coefficient, and endothermic chemical reactions, $Q < 0$ represents heat absorption coefficient and $K_m$ denotes the reaction rate constant of the $m^{\text{th}}$ order homogeneous and irreversible reaction. To obtain the similarity transformation, a special form $B_0(x)$, $Q(x)$ and $K_m(x)$ are considered and are defined as

$$B_0(x) = B_0 x^{(n-1)/2}, \quad Q(x) = Q\, x^{n-1} \text{ and } \quad K_m(x) = K_m\, x^{(1-m)s+(n-1)}. \tag{6}$$

The second term in the right hand side of Eq. (3) is due to thermal buoyancy force. Further, the positive sign represents buoyancy assisting flow in the upper half of the region where, the flow due to buoyancy and stretching sheet must assist each other. On the other hand, the negative sign represents buoyancy opposing flow in the lower half of the region where, the flow due to buoyancy and stretching sheet oppose each other. The reverse phenomenon is observed when the sheet is cooled below ambient temperature. The thermo-physical transport fluid properties of the ambient fluid are assumed to be isotropic and constant, except for the fluid viscosity, the fluid thermal conductivity and the fluid species diffusivity which are assumed to vary as a function of temperature and species diffusion. Further, $\mu(T)$ is the coefficient of viscosity which varies as an inverse function of temperature, $k(T)$ is the temperature-dependent thermal conductivity and $D(C)$ is the chemical molecular diffusion coefficient of the diffusing species in the fluid and are defined as follows [36]

$$\mu^{-1} = \mu_\infty^{-1}\left[1 + \delta(T - T_\infty)\right], \tag{7}$$

$$k(T) = k_\infty\left[1 + \varepsilon_1\,\left(T - T_\infty\right)\Delta T^{-1}\right], \tag{8}$$

$$D(C) = D_\infty\left[1 + \varepsilon_2\,\left(C - C_\infty\right)\Delta C^{-1}\right], \tag{9}$$

where $\mu_\infty, k_\infty, \text{and } D_\infty$ are respectively, the ambient fluid viscosity, the thermal conductivity and the species diffusivity. $\Delta T = T_w - T_\infty$ and $\Delta C = C_w - C_\infty$ are the temperature difference and species difference respectively. Here $\varepsilon_1$ and $\varepsilon_2$ are the small parameters known as the variable thermal conductivity and the variable species diffusion parameters. Eq. (7) can be written as

$$\mu^{-1} = a\,(T - T_r), \tag{10}$$

where $a=\delta\mu_{\infty}^{-1}$ and $T_r=T_{\infty}-\delta^{-1}$. (11)

Both $a$ and $T_r$ are constants and their values depend on the reference state and the thermo-physical property of the fluid, i.e., $\delta$ is a small parameter reflecting a thermal property of the fluid: In general, $a>0$ for liquids and $a<0$ for gases. Also, $\theta_r$ is a constant which is defined as

$$\theta_r=\left(T_r-T_{\infty}\right)\Delta T^{-1}=-\left(\delta\Delta T\right)^{-1}. \tag{12}$$

$q_r$ is the radioactive flux recognized by $q=-4\sigma^{*}\left(3k^{*}\right)^{-1}T_y^4$ . The temperature differences inside flow region are small enough, therefore $T^4$ can be obtained by expanding Taylor series around $T^4$ and ignoring the terms of greater order we get $T^4\approx 4T_{\infty}{}^3T-3T_{\infty}{}^4$ .

Let the dimensionless similarity variable be

$$\eta=y\sqrt{\frac{U_0(n+1)x^{n-1}}{2\nu_{\infty}}}\ . \tag{13}$$

The dimensionless stream function $\psi(x,y)$, the temperature distribution $\theta(\eta)$ and the concentration field $\varphi(\eta)$ are defined as

$$\psi(x,y)=f(\eta)\sqrt{\frac{2}{n+1}U_0\nu_{\infty}x^{n+1}}\ ,\quad \theta(\eta)=\frac{T-T_{\infty}}{T_w-T_{\infty}},\quad \varphi(\eta)=\frac{C-C_{\infty}}{C_w-C_{\infty}} \tag{14}$$

where, the stream function $\psi(x,y)$ satisfies the continuity Eq. (2). With the use of (6) to (14), Eq. (2) to Eq. (5) reduces to

$$\left(1+\beta^{-1}\right)\left(f''\left(1-\theta\theta_r^{-1}\right)^{-1}\right)'+ff''-2n\left(n+1\right)^{-1}f'^2+Gr\,\theta+Gc\,\varphi-K_p\,f'=0, \tag{15}$$

$$\left(1+4/3\,R_d\right)\theta''+\varepsilon_1\left(\theta\theta''+\theta'^2\right)+\Pr\left[f\theta'-2r\left(n+1\right)^{-1}f'\theta\right]+\Pr\alpha\,\theta=0, \tag{16}$$

$$\left[(1+\varepsilon_2\varphi)\varphi'\right]'+Sc\left[f\varphi'-2s\left(n+1\right)^{-1}f'\varphi\right]-Sc\,\gamma\,\varphi^m=0. \tag{17}$$

These systems of equations are subjected to the following dimensionless boundary conditions

$$\begin{aligned} &f(\eta)=0,\ f'(\eta)=1,\ \theta(\eta)=1,\ \varphi(\eta)=1 \quad at\quad \eta=0,\\ &f'(\eta)=0,\ \theta(\eta)=0,\ \varphi(\eta)=0 \quad as\quad \eta\to\infty. \end{aligned} \tag{18}$$

Here $f$ , $\theta$ and $\varphi$ are the dimensionless velocity, temperature and species diffusion fields respectively. The parameters $\theta_r$, $K_p$, $Gr$, $Gc$, $\Pr$, $\alpha$, $Sc$, $\gamma$ and $R_d$ are respectively, the fluid viscosity parameter, the permeability parameter, the local Grashof number, the local solute Grashof

number (mixed convection parameters), the Prandtl number, the modified heat source /sink parameter, the Schmidt number, the reaction rate parameter and the radiation parameter. These parameters are defined as

$$\theta_r = \frac{T_r - T_\infty}{T_w - T_\infty}, \qquad K_p = \frac{\mu_\infty}{K_p^* U_0}, \qquad Gr = \frac{2g\beta_T (T_w - T_\infty)}{(n+1)U_0^2 x^{2n-1}}, \qquad Gc = \frac{2g\beta_C (C_w - C_\infty)}{(n+1)U_0^2 x^{2n-1}},$$

$$\Pr = \frac{\mu_\infty C_p}{k_\infty}, \quad \alpha = \frac{2Q}{(n+1)\rho_\infty C_p U_0}, \quad Sc = \frac{\nu_\infty}{D_\infty} \quad and \quad \gamma = \frac{2K_m B^{m-1}}{(n+1)U_0}, \quad R_d = \frac{16\sigma^*}{3k^*} T_\infty^{\,3}.$$

Here $Gr$ and $Gc$ are the functions of $x$. To make both $Gr$ and $Gc$ independent of *x* we consider $r = s = 2n-1$. Thus, the similarity solutions are obtained under this limitation when $Gr = Gc = 0$. We notice that when $r = 2n-1$, $Gr$ is a constant, with $Gr > 0$ and $Gr < 0$ correspond to the assisting flow and opposing flow, respectively, while $Gr = 0$ (i.e. $T_w = T_\infty$) represents the case when the buoyancy force is absent (pure forced convection flow). From the mass diffusion Eq. (17), we can see the following three cases

(i) $\gamma > 0$, imply the destructive chemical reaction;
(ii) $\gamma = 0$, imply no chemical reaction; and
(iii) $\gamma < 0$, imply the generative chemical reaction.

The quantities with core physical interest are skin friction coefficient $C_{fx}$, Nusselt number $Nu_x$ and Sherwood number $Sh_x$ and are defined as

$$C_{f_x} = \frac{2\sqrt{(n+1)/2}\ \theta_r}{(\theta_r - 1)} \left(\mathrm{Re}_x\right)^{-1/2} f''(0),$$

$$Nu_x = -\sqrt{(n+1)/2}\ (1+\varepsilon_1)\left(\mathrm{Re}_x\right)^{1/2} \theta'(0) \text{ and}$$

$$Sh_x = -\sqrt{(n+1)/2}\ (1+\varepsilon_2)\left(\mathrm{Re}_x\right)^{1/2} \phi'(0).$$

### 3. Semi-analytical Solution: Optimal Homotopy Analysis Method (OHAM)

The optimal homotopy analysis method has been employed to solve the following nonlinear system of Eq. (15) to Eq. (17). Mathematica software is used obtain the analytical results for higher order approximations. In accordance with the boundary conditions (18), consider the base functions as $\{e^{(-n\eta)}\ for\ n \geq 0\}$ then, the dimensionless velocity $f(\eta)$, temperature $\theta(\eta)$ and concentration $\varphi(\eta)$ can be expressed in the series form as follows

$$f(\eta) = \sum_{n=0}^{\infty} a_n e^{(-n\eta)}, \quad \theta(\eta) = \sum_{n=0}^{\infty} b_n e^{(-n\eta)} \text{ and } \varphi(\eta) = \sum_{n=1}^{\infty} c_n e^{(-n\eta)}$$

where $a_n, b_n$ and $c_n$ are the coefficients. According to the rule of solution expression and boundary conditions (18), we assume the following:

(a) Initial guesses for dimensionless velocity $f(\eta)$ and temperature $\theta(\eta)$ and concentration $\varphi(\eta)$ [1-38]

$f_0(\eta) = 1 - e^{-\eta}$, $\theta_0(\eta) = e^{-\eta}$ and $\varphi_0(\eta) = e^{-\eta}$.

(b) Linear operators $L_1$, $L_2$ and $L_3$ as

$L_1() = \frac{d^3()}{d\eta^3} - \frac{d()}{d\eta}$, $L_2() = \frac{d^2()}{d\eta^2} + \frac{d()}{d\eta}$ and $L_3() = \frac{d^2()}{d\eta^2} + \frac{d()}{d\eta}$ such that

$L_1[c_1 + c_2 e^{\eta} + c_3 e^{-\eta}] = 0, L_2[c_4 + c_5 e^{-\eta}] = 0$ and $L_3[c_6 + c_7 e^{-\eta}] = 0$

where $c_i$'s $(i = 1, 2, 3, 4, 5, 6, 7)$ are arbitrary constants.

(c) Auxiliary function as $H_1(\eta) = e^{-\eta}, H_2(\eta) = e^{-\eta}$ and $H_3(\eta) = e^{-\eta}$ .

Let us consider so called zero[th] order deformation equation

$$(1-q)L_1\left[\hat{f}(\eta,q) - f_0(\eta)\right] = qH_1(\eta)\bar{h}N_1\left[\hat{f}(\eta,q), \hat{\theta}(\eta,q), \left(\hat{\varphi}(\eta,q)\right)\right],$$

$$(1-q)L_2\left[\hat{\theta}(\eta,q) - \theta_0(\eta)\right] = qH_2(\eta)\bar{h}N_2\left[\hat{\theta}(\eta,q), \hat{f}(\eta,q)\right],$$

$$(1-q)L_3\left[\hat{\varphi}(\eta,q) - \varphi_0(\eta)\right] = qH_3(\eta)\bar{h}N_3\left[\hat{\varphi}(\eta,q), \hat{f}(\eta,q)\right],$$

with conditions

$$\hat{f}(0,q) = 0,\ \hat{f}'(0,q) = 1,\ \hat{f}'(\infty,q) = 0;\ \hat{\theta}(0,q) = 1,\ \hat{\theta}(\infty,q) = 0;\ \hat{\varphi}(0,q) = 1,\ \hat{\varphi}(\infty,q) = 0.$$

where $q \in [0,1]$ is an embedding parameter, $\bar{h} \neq 0$ is the convergence control parameter and $N_1, N_2$ and $N_3$ are nonlinear operators.
Hence, by defining

$$f_m(\eta) = \frac{1}{m!}\frac{d^m f(\eta,q)}{d\eta^m}\bigg|_{q=0}, \theta_m(\eta) = \frac{1}{m!}\frac{d^m \theta(\eta,q)}{d\eta^m}\bigg|_{q=0}, \varphi_m(\eta) = \frac{1}{m!}\frac{d^m \varphi(\eta,q)}{d\eta^m}\bigg|_{q=0}$$

we expand $\hat{f}(\eta,q)$, $\hat{\theta}(\eta,q)$ and $\hat{\varphi}(\eta,q)$ by means of Taylor's series as

$$\hat{f}(\eta,q)=f_0(\eta)+\sum_{m=1}^{\infty}f_m(\eta)q^m,\ \hat{\theta}(\eta,q)=\theta_0(\eta)+\sum_{m=1}^{\infty}\theta_m(\eta)q^m \text{ and}$$
$$\hat{\varphi}(\eta,q)=\varphi_0(\eta)+\sum_{m=1}^{\infty}\varphi_m(\eta)q^m. \quad (19)$$

If the series (19) converges at $q=1$, we get the homotopy series solution as

$$f(\eta)=f_0(\eta)+\sum_{m=1}^{\infty}f_m(\eta),\ \theta(\eta)=\theta_0(\eta)+\sum_{m=1}^{\infty}\theta_m(\eta) \text{ and } \varphi(\eta)=\varphi_0(\eta)+\sum_{m=1}^{\infty}\varphi_m(\eta). \quad (20)$$

It should be noted that $f(\eta),\ \theta(\eta) \text{ and } \varphi(\eta)$ in Eq. (20) contain an unknown convergence control parameter $\bar{h}\neq 0$, which can be used to adjust and control the convergence region and the rate of convergence of the homotopy series solution.

Now we evaluate the error and minimize over $\bar{h}$ in order to obtain the optimal value of $\bar{h}$ and least possible error. At $m^{th}$ order deformation equation, the average residual error defined as

$$E_m{}^{f}(\bar{h})=\frac{1}{M+1}\sum_{k=0}^{M}\left(N_1\left[\sum_{n=0}^{m}f_n(\eta_k)\right]\right)^2,\ E_m{}^{\theta}(\bar{h})=\frac{1}{M+1}\sum_{k=0}^{M}\left(N_2\left[\sum_{n=0}^{m}\theta_n(\eta_k)\right]\right)^2 \text{ and}$$

$$E_m{}^{\varphi}(\bar{h})=\frac{1}{M+1}\sum_{k=0}^{M}\left(N_3\left[\sum_{n=0}^{m}\varphi_n(\eta_k)\right]\right)^2$$

where $\eta_k=k\Delta\eta=\frac{k}{M},k=0,1,2,....M$ and M=20 for Blasius flow problem.

Now the error function $E_m{}^{f}(\bar{h})$, $E_m{}^{\theta}(\bar{h})$ and $E_m{}^{\varphi}(\bar{h})$ is minimized in $\bar{h}$ to obtain the optimal value of $\bar{h}$. Substituting this optimal value of $\bar{h}$ in Eq. (20) we get the approximate solutions of Eq. (15) to Eq. (17), which satisfies the conditions (18).

In order to validate the method used, the values of $-f''(0)$ obtained by OHAM are comparison with the exact solution which is well known when $n=1, Gr=Gc=K_p=0$ and $\theta r\to\infty$ and also the wall temperature gradient results have been compared with the previously published papers of Prasad *et al.,* [36], Vajravelu *et al.,* [39], Ishak *et al.,* [40], and Ali [41] for several special cases and the results are found to be in good agreement: The results are shown in Table 1 and Table 2.

**Table 1**
Comparison between exact and analytical solution by OHAM for $-f''(0)$ when $n=1, Gr=Gc=K_p=0$ and $\theta r \to \infty$

| $\beta$ | Exact solution | OHAM Solution (13th Approximation) | Relative error |
|---|---|---|---|
| $\infty$ | -1.0000 | -1.0000 | 0 |
| 1.0 | -0.70710678 | -0.707108 | 0.0000017253 |
| 2.0 | -0.81649658 | -0.816497 | 0.0000005143 |
| 3.0 | -0.866025414 | -0.866025 | 0.0000004780 |
| 4.0 | -0.894427191 | -0.894427 | 0.0000002135 |
| 5.0 | -0.912870929 | -0.912871 | 0.0000000777 |

**Table 2**
Comparison of wall temperature gradient $\theta'(0)$ for different values of $\mathrm{Pr}$, $Gr$ and $\varepsilon_1$ when $\beta \to \infty, \theta_r \to \infty, n=1.0, Gc=0.0, Mn=0.0$ and $\alpha=0.0$

| Pr | $Gr$ | $\varepsilon_1$ | Vajravelu *et al.*, [39] | Ishak *et al.*, [40] | Ali [41] | Prasad *et al.*, [36] | Present result |
|---|---|---|---|---|---|---|---|
| 1.0 | 1.0 | 0.1 | -1.018446 | - | - | -1.018290 | -1.018270 |
| | | 0.0 | -1.087206 | -1.087300 | - | -1.087020 | -1.087050 |
| | 2.0 | 0.0 | -1.142298 | -1.142300 | - | -1.143300 | -1.143340 |
| | 3.0 | | -1.185197 | -1.185300 | - | -1.186900 | -1.186940 |
| 0.72 | 0.0 | 0.0 | -0.808836 | -0.808600 | -0.805800 | -0.815699 | -0.815689 |
| 1.0 | | | -1.000000 | -1.000000 | -0.996100 | -1.000000 | -1.000000 |
| 3.0 | | | -1.923687 | -1.923700 | -1.914400 | -1.923930 | -1.923950 |
| 10.0 | | | -3.720788 | -3.720700 | -3.700600 | -3.720420 | -3.720410 |

## 4. Results and Discussion

Obtaining analytical solutions for the highly nonlinear and coupled system (15) to (17) with the boundary condition (18) is a challenging task. However, this can be achieved by utilizing the Optimal Homotopy Analysis Method (OHAM), a powerful analytical technique introduced by Liao [1] and further developed by Fan and You [38]. With the help of OHAM, the solutions for the system can be obtained accurately and efficiently. The results for the velocity field $f'(\eta)$, the temperature field $\theta(\eta)$, and the concentration field $\varphi(\eta)$ are presented for different values of the Casson parameter $\beta$, the variable viscosity parameter $\theta_r$, the Prandtl number $\mathrm{Pr}$, the permeability parameter $K_p$, the modified heat source/sink parameter $\alpha$, the thermal conductivity parameter $\varepsilon_1$, the variable species diffusivity parameter $\varepsilon_2$, the local Grashof number $Gr$, the local solute Grashof number $Gc$, the velocity exponent parameter $n$, the Schmidt number $Sc$, the reaction rate parameter $\gamma$ and the Radiation parameter $R_d$ in Figure 2 to Figure 10. It can be seen from these graphs that for all three fields $f'(\eta), \theta(\eta)$ and $\varphi(\eta)$ the profiles decrease monotonically and tends asymptotically to zero as the distance increases from the boundary. The computed values for the skin-friction coefficient $f''(0)$, the Nusselt number $\theta'(0)$ and the Sherwood number $\varphi'(0)$ are tabulated in Table 3. The validity and the accuracy of the OHAM solutions are analyzed through residual errors and are presented in Figure 11.

Figure 2(a) through Figure 2(c) elucidate the effect of increasing values of $Gr$ [-1, 0, 0.5, 1, 2] on $f'(\eta), \theta(\eta)$ and $\varphi(\eta)$. It is observed that $f'(\eta)$ increases as $Gr$ increases and hence the momentum boundary layer thickness increases which in turn enhances the velocity field. Physically, $Gr > 0$ corresponds to assisting flow, $Gr < 0$ opposing flow, and $Gr = 0$ indicates the absence of buoyancy

force> However, the effect of $Gr$ on temperature and concentration profile is quite opposite. In the case of $\theta(\eta)$ and $\varphi(\eta)$ the effect of increasing values of $Gr$ is quite opposite. A similar trend can be seen in the case of $Gc$ [-0.5, 0, 0.5, 2] also (see Figure 3(a) to Figure 3(c)). This observation is even true in the cases of $f''(\eta)$, $\theta'(\eta)$ and $\varphi'(\eta)$ (see Table 3 for details). The effect $\theta_r$ on $f'(\eta)$ is depicted in the Figure 4(a). As $\theta_r$ increases from -10.0 to -1.0, the velocity profile decrease. That is, as $\theta_r \to 0$, the momentum boundary layer thickness decreases and the velocity distribution becomes linear for higher values of $n$. Figure 4(b) and Figure 4(c) display the effect of $\theta_r$ on temperature and concentration profiles. From Eq. (12) it is clear that for higher values of $\theta_r$, $(T_w - T_\infty)$ is small, so that the effect of variable viscosity on the fluid flow is negligible and hence can be neglected but when $\theta_r$ is small, the effect of variable viscosity is prominent and cannot be neglected. Therefore, the thermal and concentration boundary layer thickness increases as $\theta_r$ increases. Figure 5(a) to Figure 5(c) exhibit the effect of $n$ on $f'(\eta)$, $\theta(\eta)$ and $\varphi(\eta)$ for different values of $\beta$. Velocity, temperature and concentration profile are found to decrease with increasing $n$ [0.5, 1, 2, 5, 10], this is because the coefficient $2n/(n+1)$ in Eq. (15) approaches 2 as $n \to \infty$. Here it is worth noting that the effect of $n$ is significant when $n$ is very less and is highly negligible when $n$ is very large. Further, it is observed that fluid velocity is much more suppressed in the case of $\beta \to \infty$ than that of $\beta = 2.0$ (see Figure 5(a)), and is quite the opposite in the case of temperature and concentration profiles. This leads to a thinner momentum boundary and a thicker thermal and concentration boundary layer as $\beta$ increases. Figure 6(a) to Figure 6(c) explains the effect of the permeability parameter $K_p$ [0, 0.5, 1, 1.5] on velocity, temperature and concentration profile respectively. With increasing permeability parameter, the resistance to the fluid motion increases and hence velocity decreases, and the opposite behavior is seen in temperature and concentration profiles. The permeability parameter $K_p$ grows a resistance force (due to the increase in the pores in the fluid) that works conversely to the flow field and enhances the thermal and solutal boundary layer thickness.

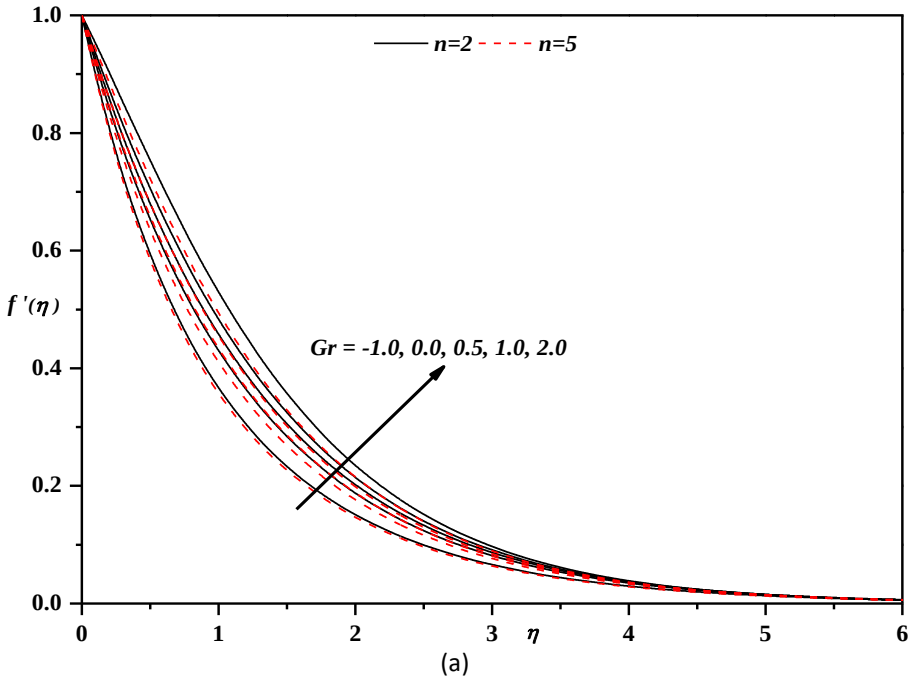

(a)

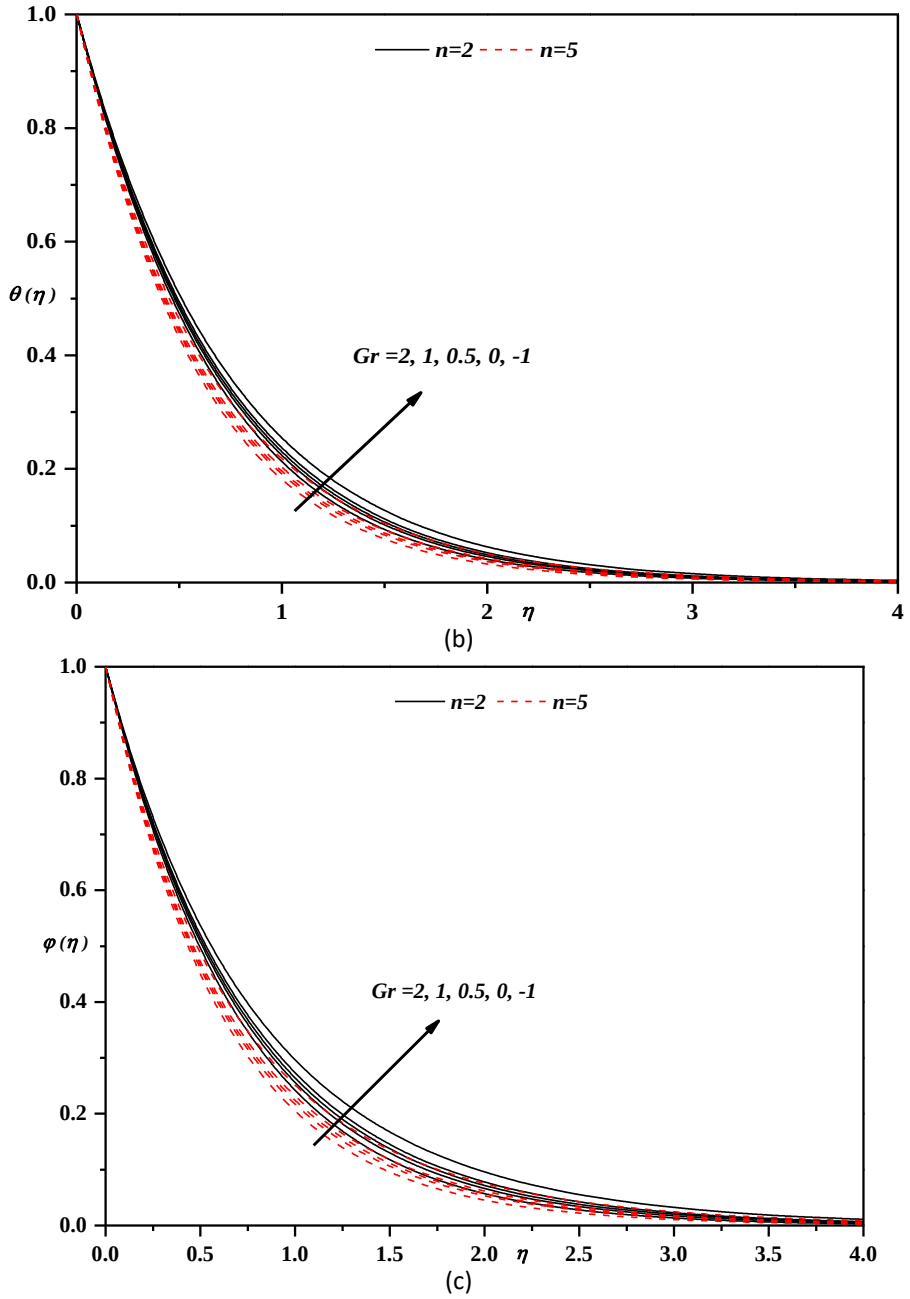


**Fig. 2.** (a) Horizontal velocity profile, (b) temperature profile, (c) concentration profile for different values of $Gr$ and $n$ with $Pr = 1.0$, $Sc = 1.0$, $\varepsilon_1 = 0.2$, $\varepsilon_2 = 0.2$, $\beta = 1.0$, $\theta_r = -10.0$, $Mn = 0.5$, $Gc = 0.5$, $\delta = 0.5$, $\alpha = -0.5$, $m = 2$, $K_p = R_d = 0.1$

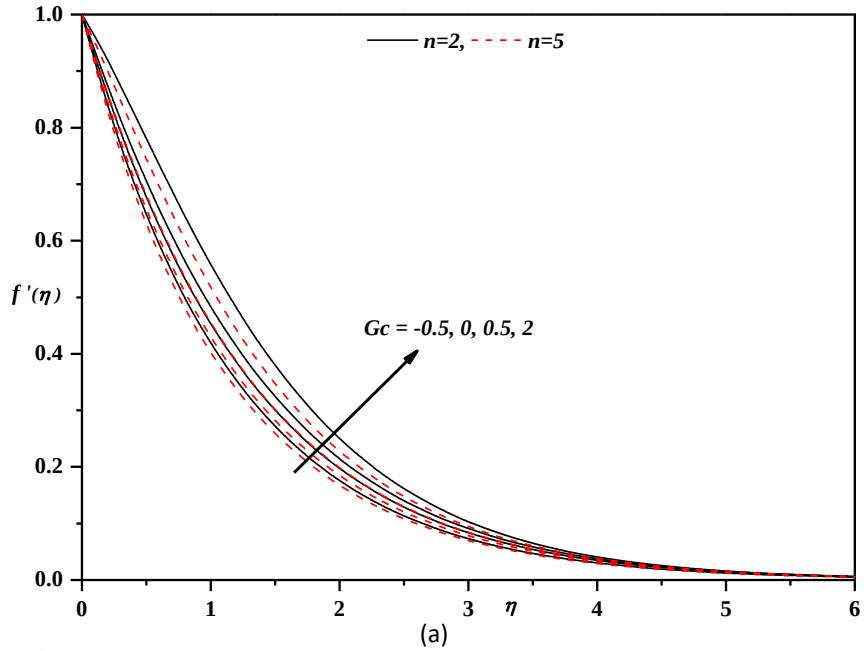
n=2, n=5
Gc = -0.5, 0, 0.5, 2
f '(η)
η
1.0
0.8
0.6
0.4
0.2
0.0
0
1
2
3
4
5
6

(a)

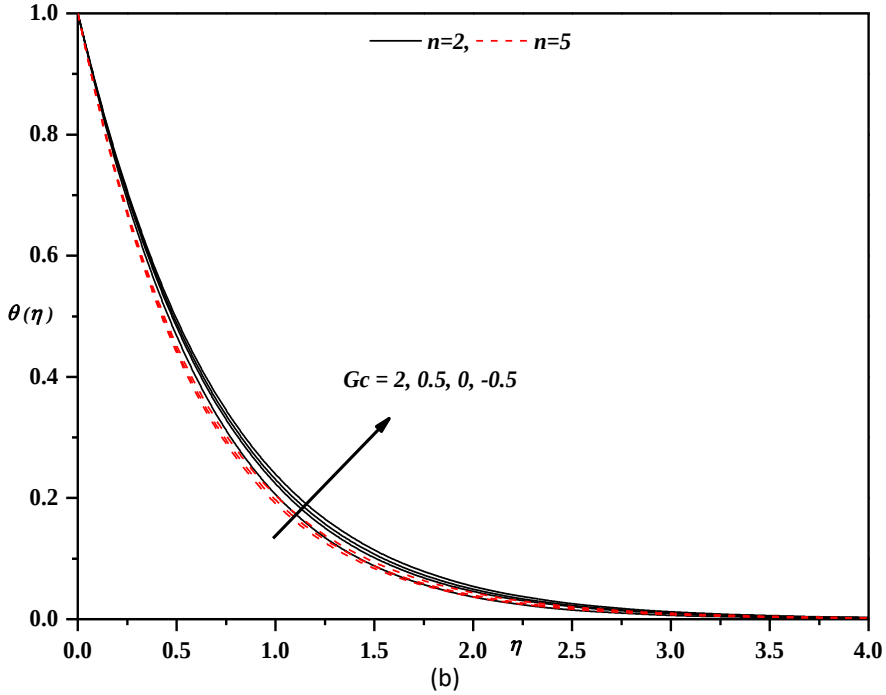
n=2, n=5
Gc = 2, 0.5, 0, -0.5
θ(η)
η
1.0
0.8
0.6
0.4
0.2
0.0
0.0
0.5
1.0
1.5
2.0
2.5
3.0
3.5
4.0

(b)

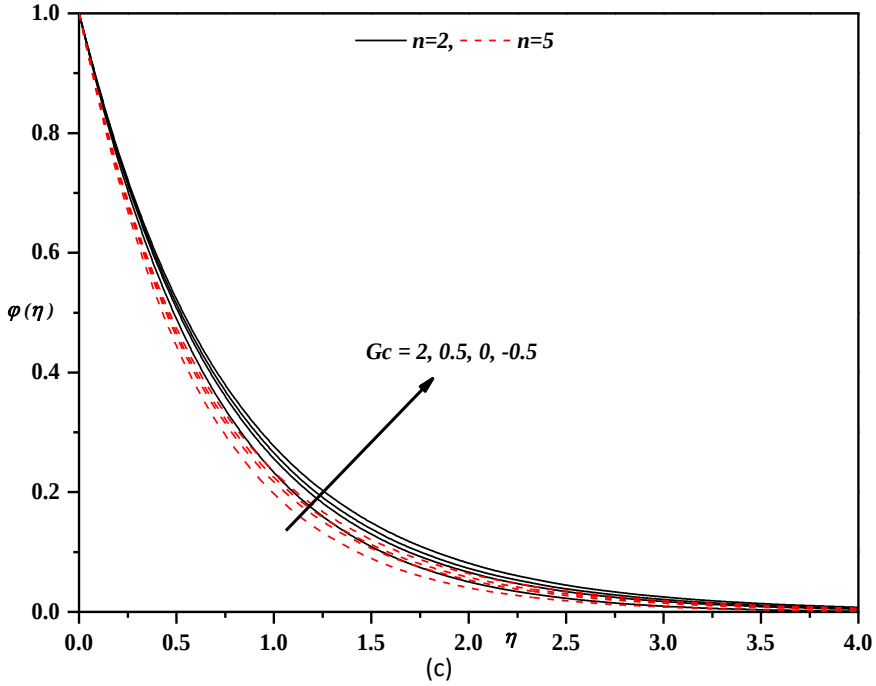


(c)

**Fig. 3.** (a) Horizontal velocity profile, (b) temperature profile, (c) concentration profile for different values of $Gc$ and $n$ with $Pr = 1.0$, $Sc = 1.0$, $\varepsilon_1 = 0.2$, $\varepsilon_2 = 0.2$, $\beta = 1.0$, $\theta_r = -10.0$, $Mn = 0.5$, $Gr = 1.0$, $\delta = 0.5$, $\alpha = -0.5$, $m = 2.0$, $K_p = R_d = 0.1$

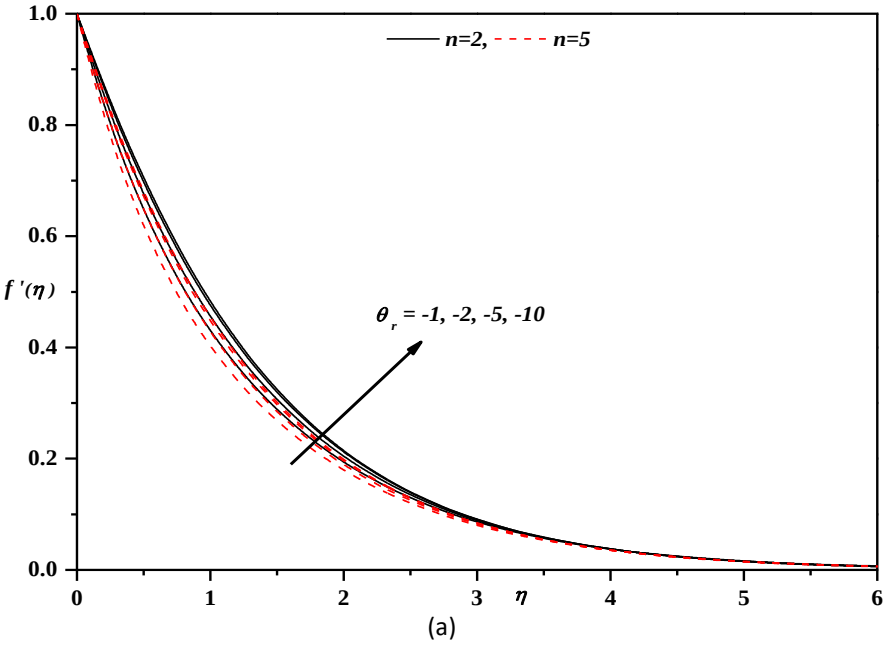


(a)

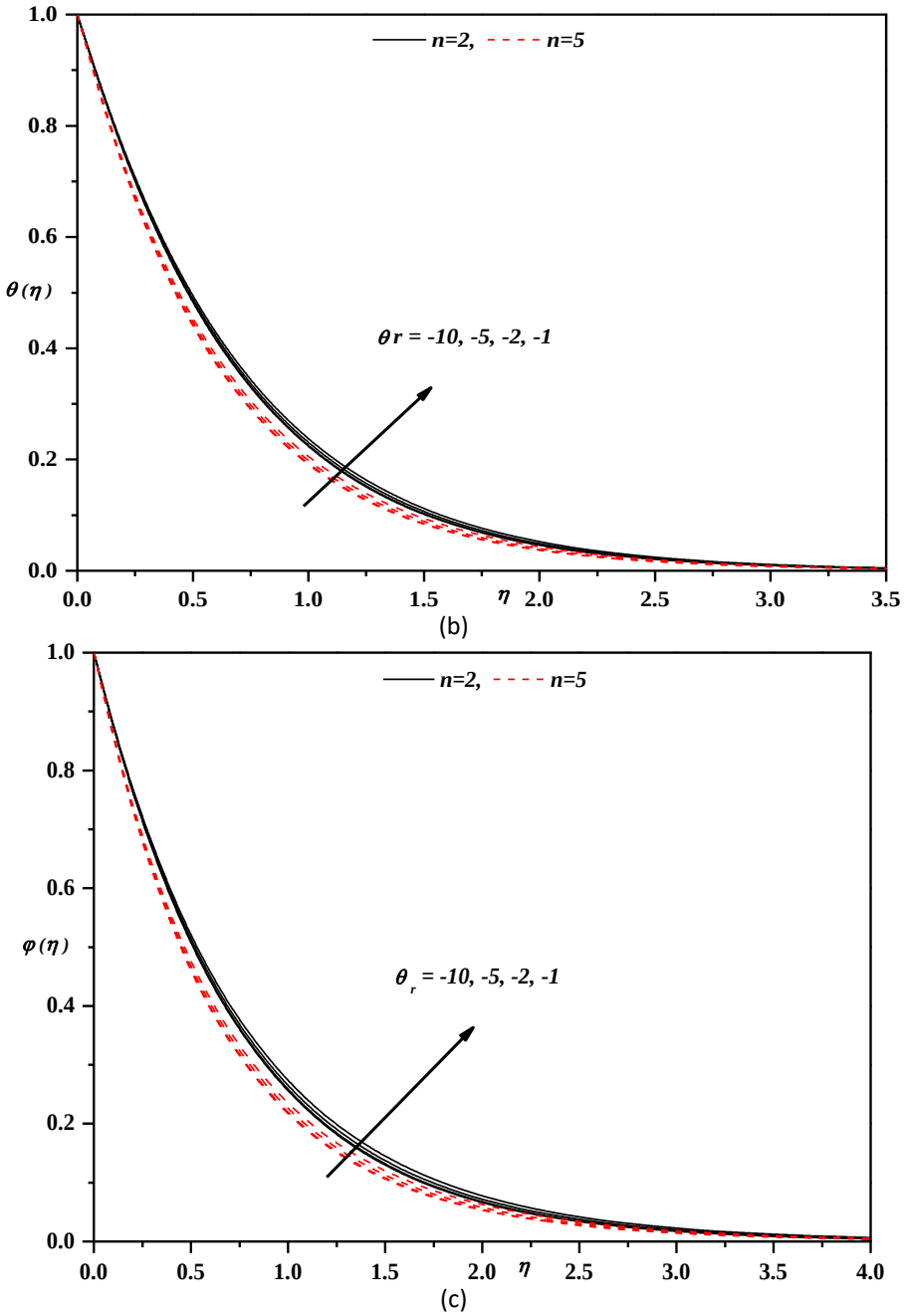


**Fig. 4.** (a) Horizontal velocity profile, (b) temperature profile, (c) concentration profile for different values of $\theta_r$ and $n$ with $Pr = 1.0$, $Sc = 1.0$, $\varepsilon_1 = 0.2$, $\varepsilon_2 = 0.2$, $\beta = 1.0$, $Gc = 0.5$, $Mn = 0.5$, $Gr = 1.0$, $\delta = 0.5$, $\alpha = -0.5$, $m = 2.0$, $K_p = R_d = 0.1$

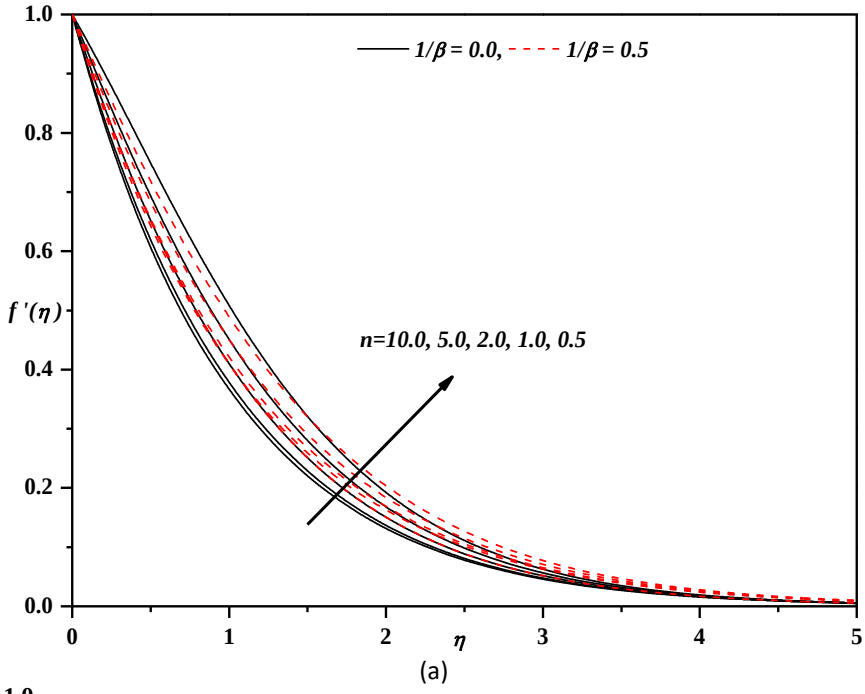
1.0
0.8
0.6
0.4
0.2
0.0
f '(η)
1/β = 0.0, 1/β = 0.5
n=10.0, 5.0, 2.0, 1.0, 0.5
0
1
2
3
4
5
η

(a)

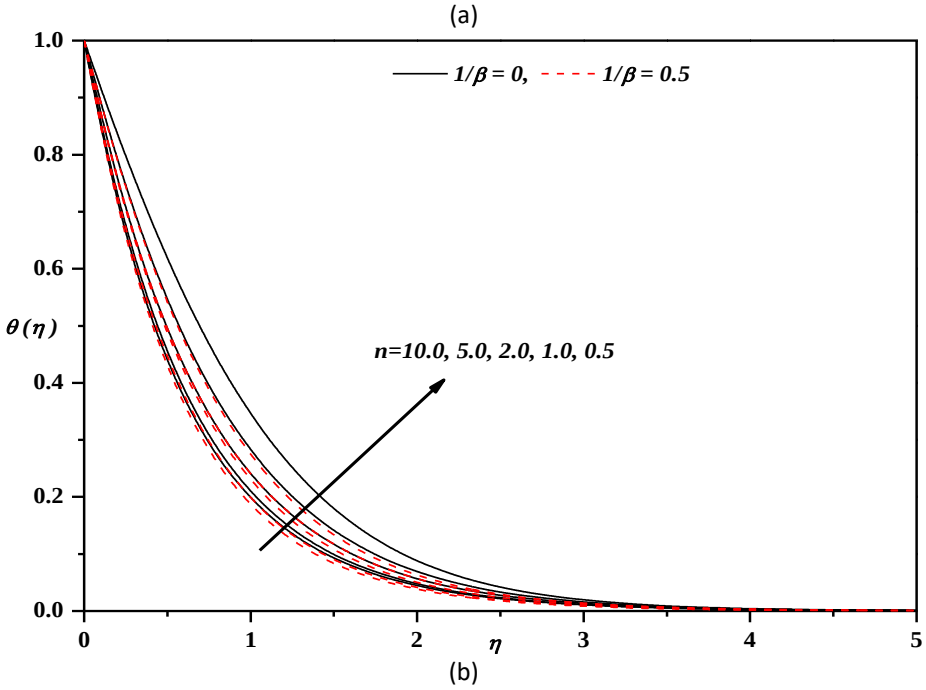
1.0
0.8
0.6
0.4
0.2
0.0
θ(η)
1/β = 0, 1/β = 0.5
n=10.0, 5.0, 2.0, 1.0, 0.5
0
1
2
3
4
5
η

(b)

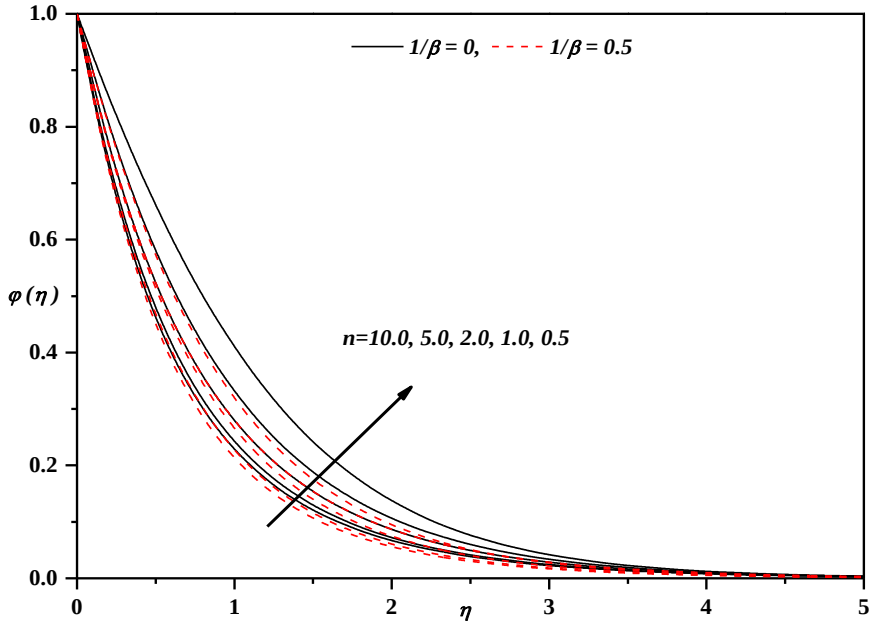


(c)

**Fig. 5.** (a) Horizontal velocity profile, (b) temperature profile, (c) concentration profile for different values of $\beta$ and $n$ with $Pr = 1.0$, $Sc = 1.0$, $\varepsilon_1 = 0.2$, $\varepsilon_2 = 0.2$, $\theta_r = -10.0$, $Gr = 1.0$, $Gc = 0.5$, $Mn = 0.5$, $\alpha = -0.5$, $\delta = 0.5$, $m = 2.0$, $K_p = R_d = 0.1$

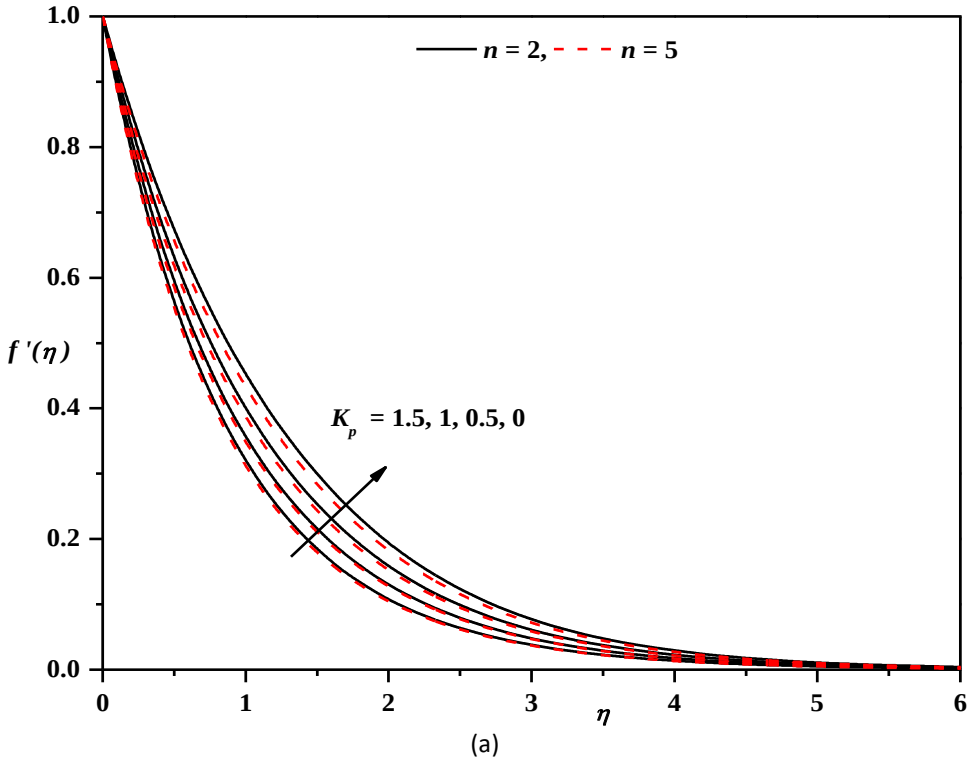


(a)

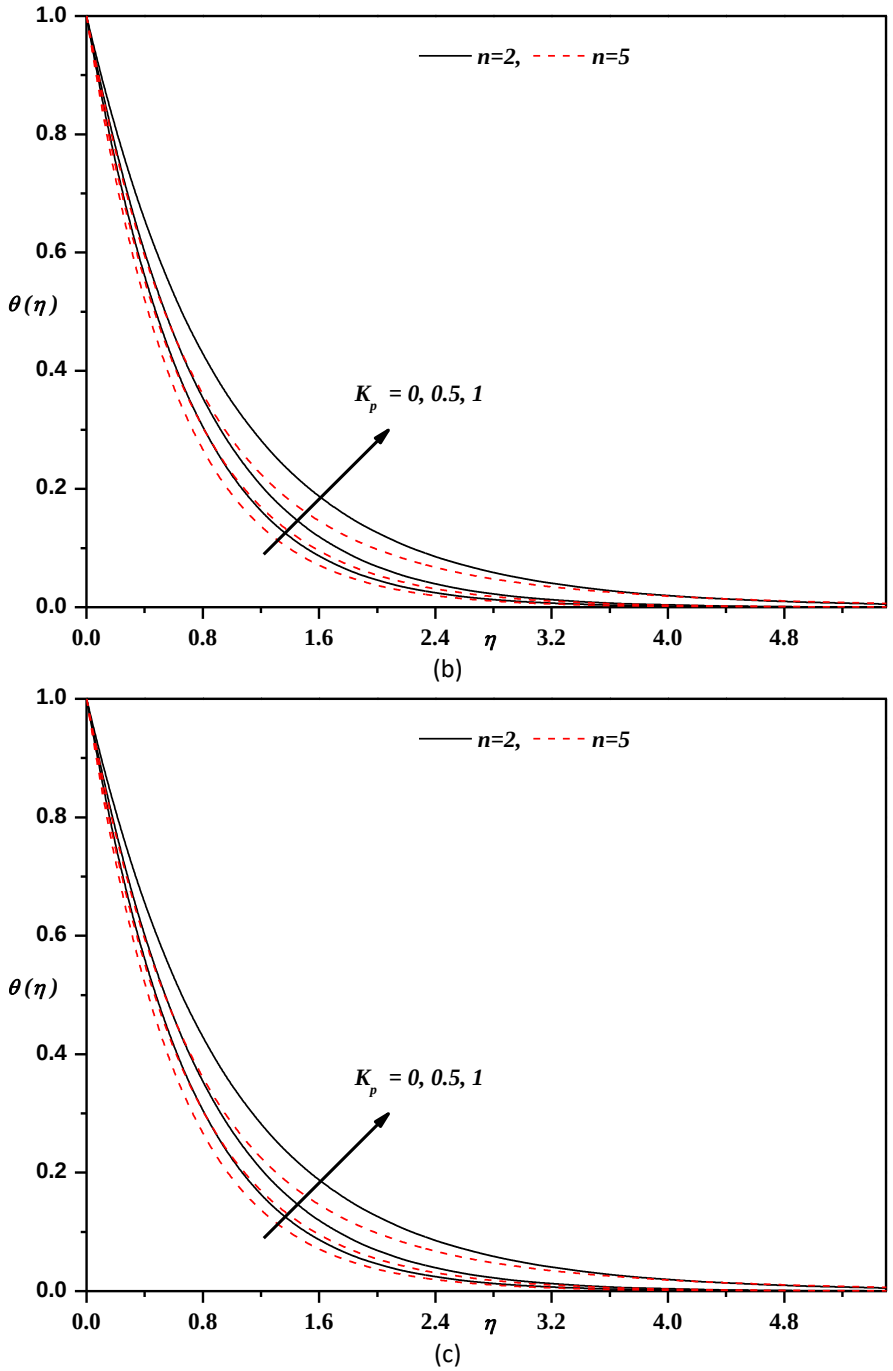


**Fig. 6.** (a) Horizontal velocity profile, (b) temperature profile, (c) concentration profile for different values of $K_p$ and $n$ with $Sc = 1.0$, $\varepsilon_1 = \varepsilon_2 = 0.5$, $\beta = 1.0$, $\theta_r = -10.0$, $Gc = 0.5$, $Pr = Gr = 1.0$, $Mn = 0.5$, $\delta = 0.5$, $\alpha = -0.5$, $m = 2.0$, $R_d = 0.1$

The effect of increasing value of Pr [0.72, 1, 3] and $\varepsilon_1$ [0, 0.2, 0.4] on $\theta(\eta)$ in presented in Figure 7. As Pr increases, the temperature decreases and hence thermal boundary layer thickness decreases, while quite the opposite is true in the case of increasing $\varepsilon_1$. This is due to the assumption of temperature dependent thermal conductivity $k(T) = k_\infty \left(1 + \frac{\varepsilon_1}{\Delta T}(T - T_\infty)\right)$ in energy equation which condenses the magnitude of transverse velocity by a quantity $\partial k(T)/\partial y$. Figure 8 demonstrates the effect of $\alpha$ [-0.5, 0, 0.5] on $\theta(\eta)$. Physically, $\alpha > 0$ implies there is a transfer of heat from wall to

the flow region, due to which thermal boundary layer thickness increases and hence enhances the temperature profile. On the other hand, when $\alpha < 0$, heat transfer from the flow region to the wall, due to which thinning of thermal boundary layer occurs and consequently declines the temperature profile. Figure 9 depicts the effect of radiation parameter $R_d$. Since $R_d$ is directly proportional to the free stream temperature, as the values of $R_d$ [0.2, 0.5, 0.8] increases, the temperature profile gets enhanced and consequently, the thermal boundary layer thickness also gets enhanced. The effect of increasing values of $Sc\left(=\nu_\infty / D_\infty\right)$ and $\varepsilon_2$ is presented in Figure 10. As $Sc$ [0.66, 1, 2] increases, there is a decrease in molecular diffusivity $D_\infty$ which results in a reduction in concentration boundary layer thickness. Because of this, the concentration profile decreases with increasing values of $Sc$ [0, 0.2, 0.4] and exactly the reverse trend occurs with increase in $\varepsilon_2$.

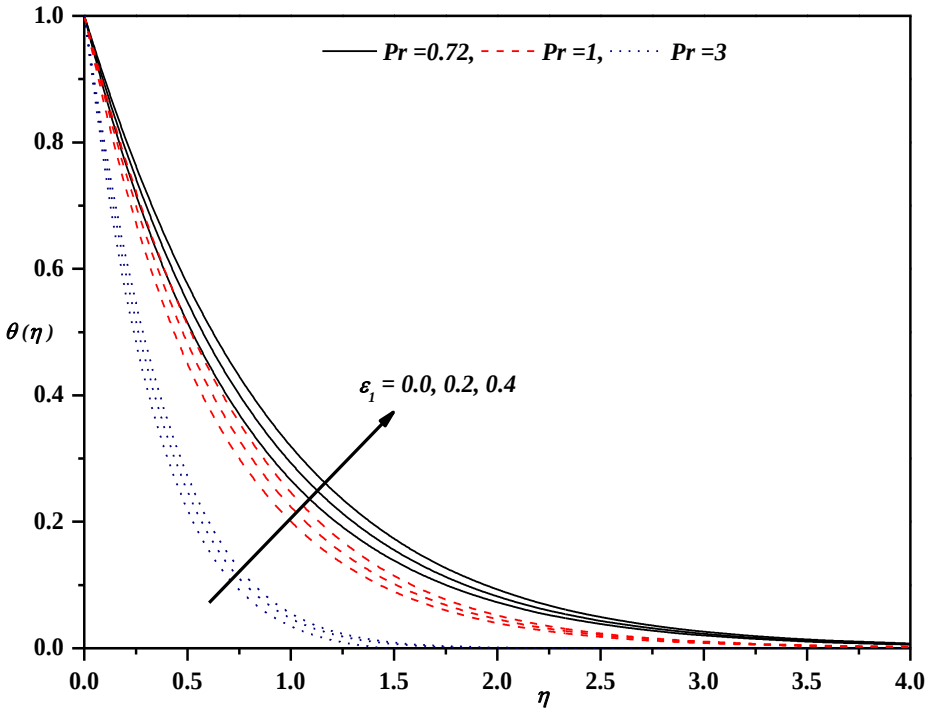


**Fig. 7.** Temperature profile for different values of $Pr$ and $\varepsilon_1$ with $Sc = 1.0$, $\varepsilon_2 = 0.5$, $\beta = 1.0$, $\theta_r = -10.0$, $Gc = 0.5$, $Gr = 1.0$, $Mn = 0.5$, $\delta = 0.5$, $\alpha = -0.5$, $m = 2.0$, $n = 2$, $K_p = R_d = 0.1$

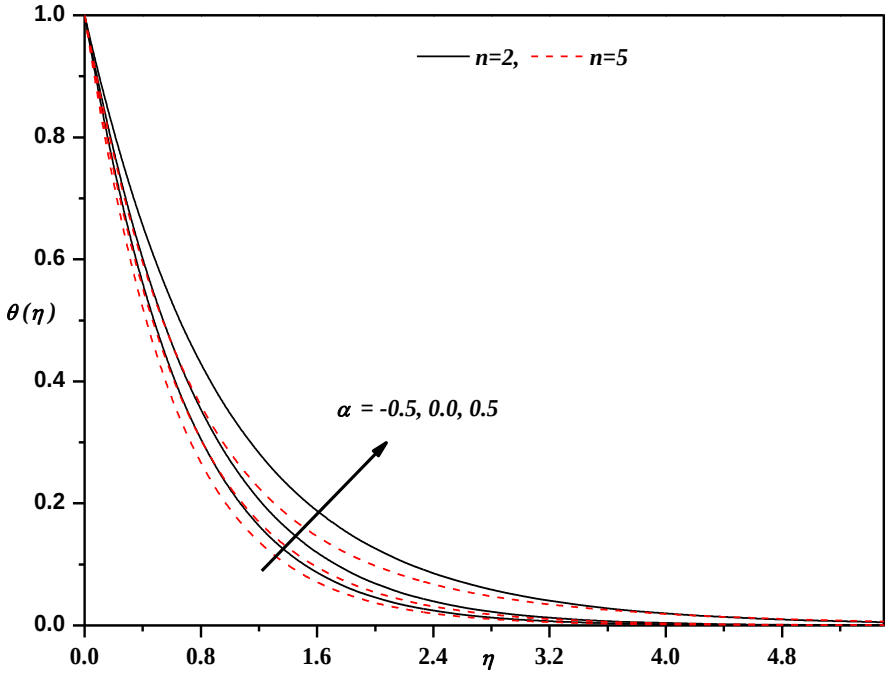


**Fig. 8.** Temperature profile for different values of $\alpha$ and $n$ with $Pr = 1.0$, $Sc = 1.0$, $\varepsilon_1 = 0.2$, $\varepsilon_2 = 0.2$, $\theta_r = -10.0$, $Gc = 0.5$, $Gr = 1.0$, $\beta = 1.0$, $Mn = 0.5$, $\delta = 0.5$, $m = 2$, $K_p = R_d = 0.1$

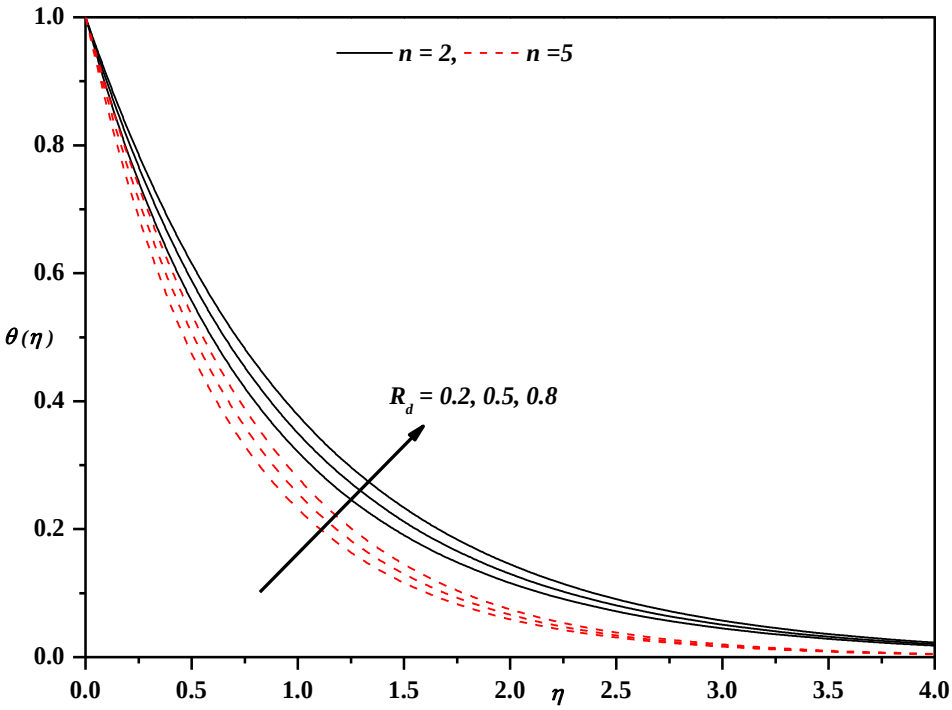


**Fig. 9.** Temperature profile for different values of $R_d$ and $n$ with $Sc = 1.0$, $\varepsilon_1 = \varepsilon_2 = 0.5$, $\beta = 1.0$, $\theta_r = -10.0$, $Gc = 0.5$, $Pr = Gr = 1.0$, $Mn = 0.5$, $\delta = 0.5$, $\alpha = -0.5$, $m = 2.0$, $K_p = 0.1$

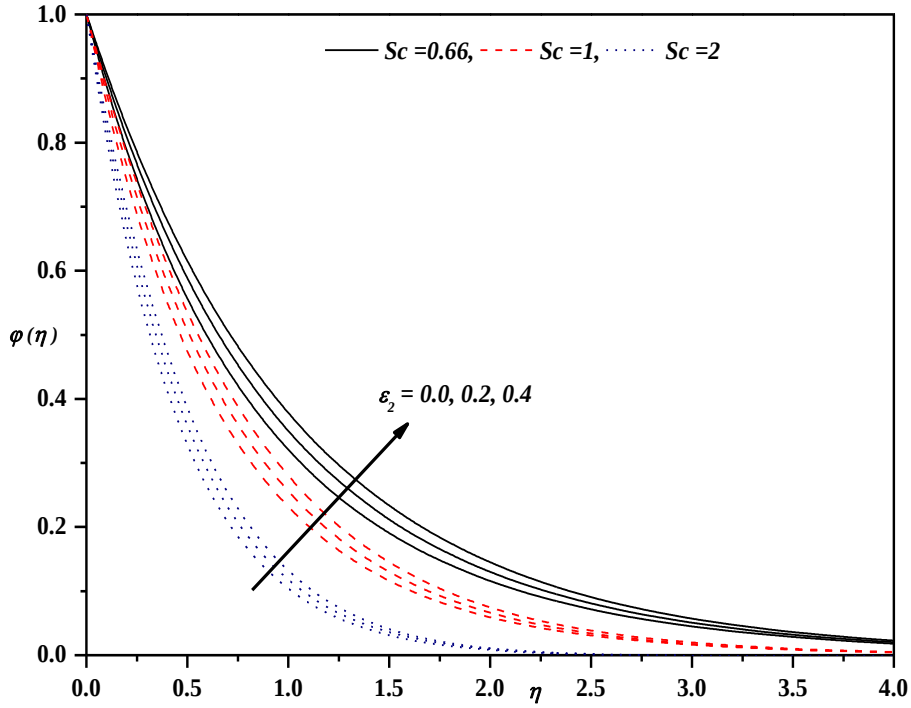


**Fig. 10.** Concentration profile for different values of $Sc$ and $\varepsilon_2$ with $Pr = 1.0$, $\varepsilon_1 = 0.5$, $\beta = 1.0$, $\theta_r = -10.0$, $Gc = 0.5$, $Gr = 1.0$, $Mn = 0.5$, $\delta = 0.5$, $\alpha = -0.5$, $m = 2.0$, $n = 2$, $K_p = R_d = 0.1$

Residual error for $f'(\eta), \theta(\eta)$ and $\phi(\eta)$ is presented in Figure 11 for two different values of *Pr* to demonstrate the accuracy and convergence of OHAM. Figure 11(a) and Figure 11(b) show that an eight-order approximation yields the best accuracy for the current problem. Figure 12(a) and Figure 12(b) are the Streamlines and 3D plots, respectively.

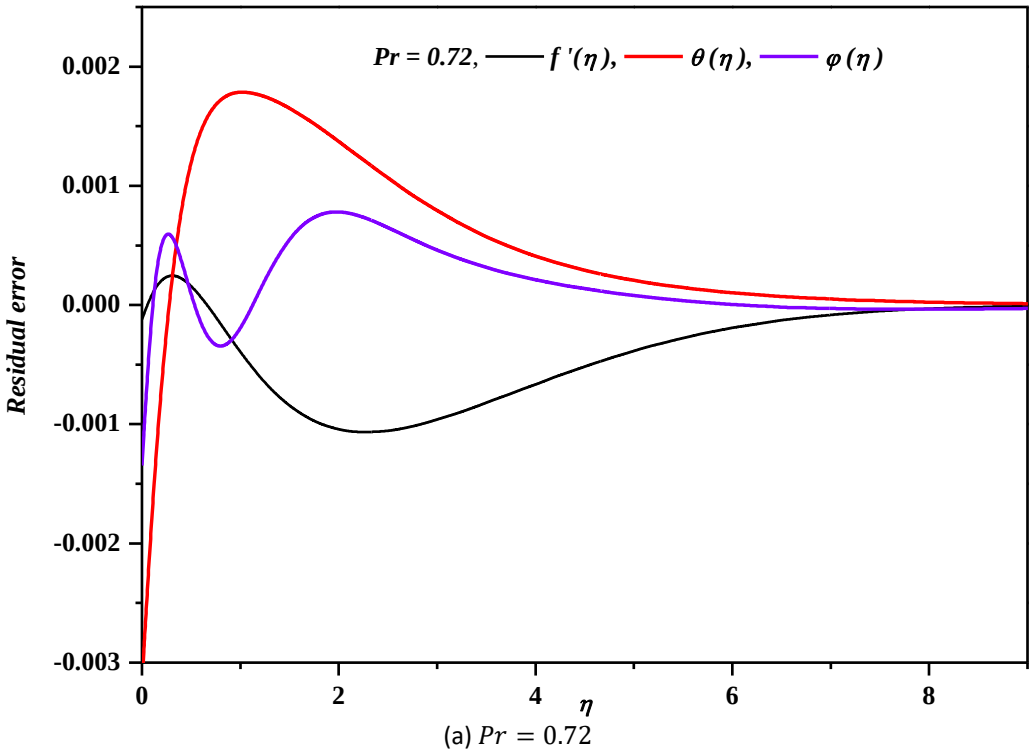


(a) $Pr = 0.72$

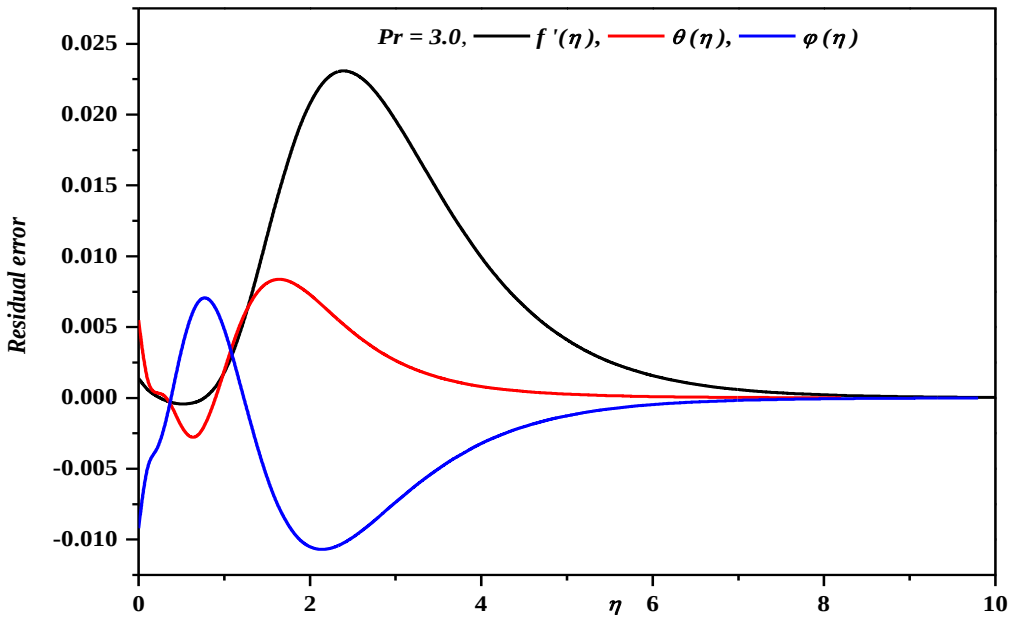


(b) $Pr = 3.0$

**Fig. 11.** Residual error profile for horizontal velocity, temperature and concentration for $\beta = 1.0$, $Sc = 1.0$, $Gr = 1.0$, $Gc = 0.5$, $\varepsilon_1 = 0.2$, $\varepsilon_2 = 0.2$, $\theta_r = -5.0$, $\delta = 0.5$, $\alpha = -0.5$, $Mn = 0.2$, $n = 2.0$, $m = 1$, $K_p = R_d = 0.1$

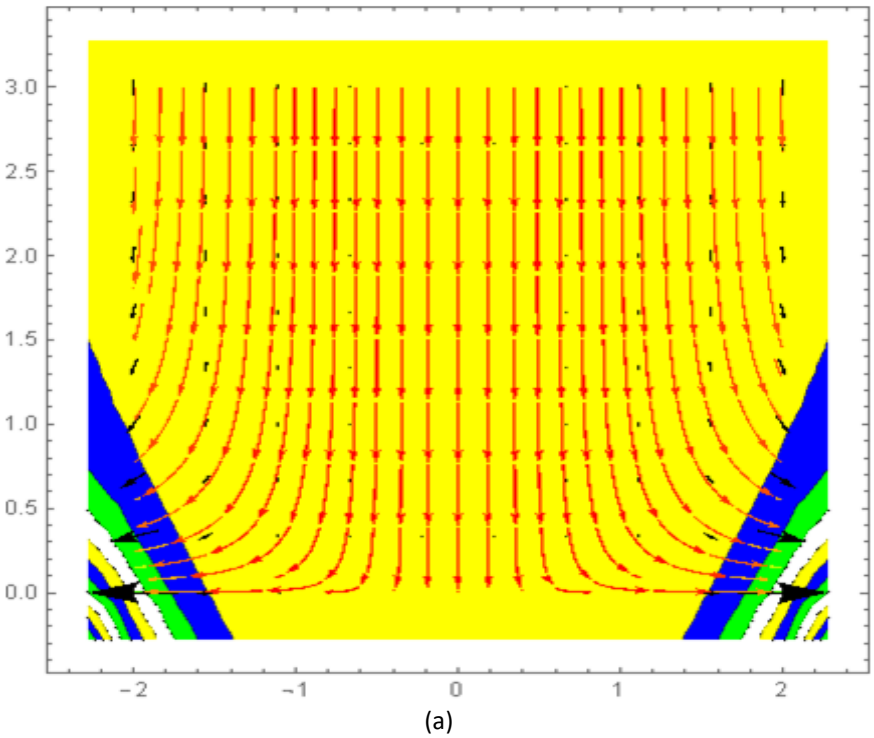


(a)

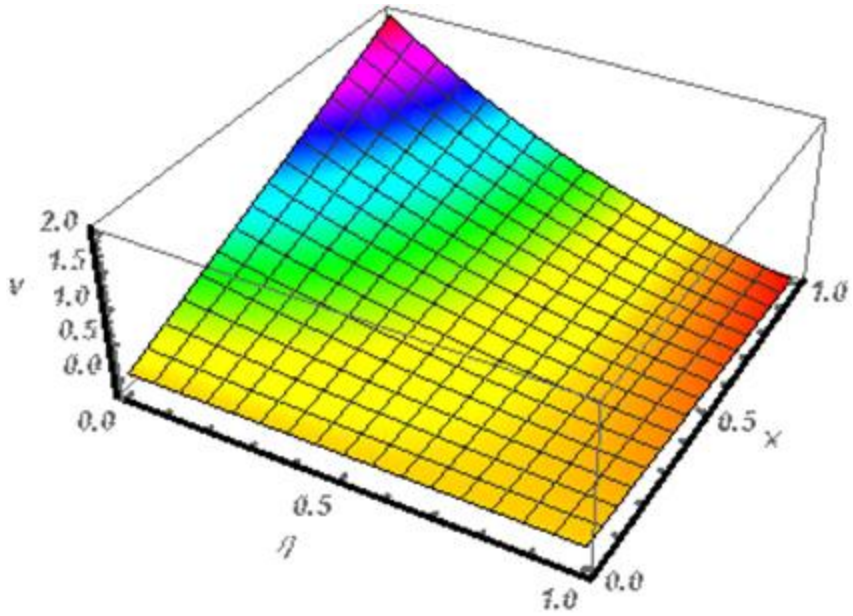


(b)

**Fig. 12.** (a) Stream density plot, (b) Three dimensional plot for $\theta_r = -5$, $n = m = 2$, $Pr = Sc = \beta = 1$, $\alpha = -0.5$, $\varepsilon_1 = \varepsilon_2 = K_p = R_d = 0.1$, $Gc = Gr = 1, Mn = \delta = 0.5$

In Table 3, we present the results for $f''(0)$, $\theta'(0)$ and $\varphi'(0)$ for several sets of values of the physical parameters. These numerical results help in better understanding of the effects of various parameters and their applications in the technological and pharmaceutical industries. For increasing values of $Gr$ and $Gc$ skin friction increases, whereas the values of the Nusselt and the Sherwood numbers decrease, and is exactly opposite in the case of $\theta_r$; but in the case of $n$ $f''(0)$, $\theta'(0)$ and $\varphi'(0)$ decrease. For increasing values of *Pr* the Nusselt number decreases but in the case of $\varepsilon_1$ it is reversed. The Sherwood number decreases for increasing values of $Sc$.

**Table 3**
Values of Skin friction, Nusselt number and Sherwood number for different values of the physical parameters

| $K_p$ | $R_d$ | Pr | $\beta$ | $\alpha$ | $\theta_r$ | $Gc$ | $Gr$ | $n=1$ | | | $n=3$ | | |
|---|---|---|---|---|---|---|---|---|---|---|---|---|---|
| | | | | | | | | $f''(0)$ | $\theta'(0)$ | $\varphi'(0)$ | $f''(0)$ | $\theta'(0)$ | $\varphi'(0)$ |
| 0.5 | 0.5 | 1.0 | 1.0 | -0.5 | -10.0 | 0.5 | 0.0 | -0.871252 | -1.383450 | -1.322500 | -0.944987 | -1.594780 | -1.541750 |
| | | | | | | | 0.5 | -0.765156 | -1.397450 | -1.334590 | -0.847351 | -1.609250 | -1.557850 |
| | | | | | | | 1.0 | -0.662781 | -1.410890 | -1.358920 | -0.753327 | -1.622650 | -1.572840 |
| | | | | | | | 2.0 | -0.463589 | -1.434480 | -1.382290 | -0.571857 | -1.646850 | -1.598950 |
| | | | | | | -0.5 | 1.0 | -0.884784 | -1.379780 | -1.317800 | -0.954156 | -1.591780 | -1.538510 |
| | | | | | | 0.0 | | -0.771787 | -1.396480 | -1.338590 | -0.852851 | -1.607140 | -1.556620 |
| | | | | | | 0.5 | | -0.662151 | -1.410450 | -1.353520 | -0.753987 | -1.622250 | -1.572420 |
| | | | | | | 2.0 | | -0.356250 | -1.448150 | -1.397860 | -0.474788 | -1.660360 | -1.613530 |
| | | | | | -10.0 | 0.5 | | -0.662251 | -1.410250 | -1.352520 | -0.753257 | -1.622980 | -1.572750 |
| | | | | | -5.0 | | | -0.696250 | -1.406360 | -1.343680 | -0.793650 | -1.617250 | -1.566860 |
| | | | | | -2.0 | | | -0.785780 | -1.396780 | -1.332840 | -0.901985 | -1.603780 | -1.551950 |
| | | | | | -1.0 | | | -0.901360 | -1.381590 | -1.323970 | -1.042210 | -1.584980 | -1.531850 |
| | | | | -0.5 | -10.0 | | | -0.662221 | -1.410150 | -1.351720 | -0.753327 | -1.622250 | -1.572750 |
| | | | | 0.0 | | | | -0.739884 | -1.483350 | -1.577890 | -0.739784 | -1.483350 | -1.575850 |
| | | | | 0.5 | | | | -0.611122 | -1.053780 | -1.369840 | -0.716983 | -1.321680 | -1.582450 |
| 0.5 | 0.5 | 1.0 | 0.5 | -0.5 | | | | -0.456253 | -0.854895 | -0.764568 | -0.814255 | -1.381480 | -1.318950 |
| | | | 1.0 | | | | | -0.654259 | -1.145250 | -1.076550 | -0.597366 | -1.157390 | -1.086850 |
| | | | 2.0 | | | | | -0.814555 | -1.381350 | -1.312170 | -0.723148 | -1.398950 | -1.338450 |
| | | | 5.0 | | | | | -0.951144 | -1.584680 | -1.523230 | -0.831789 | -1.606750 | -1.554620 |
| | | | 10.0 | | | | | -1.007180 | -1.668780 | -1.611580 | -0.877179 | -1.693950 | -1.643850 |
| 0.5 | 0.5 | 0.72 | 1.0 | | | | | -0.646257 | -1.338280 | -1.353640 | -0.635288 | -1.182850 | -1.360950 |
| | | 1.0 | | | | | | -0.673456 | -1.596350 | -1.352530 | -0.662391 | -1.410450 | -1.353850 |
| | | 3.0 | | | | | | -0.748655 | -2.855980 | -1.333470 | -0.740758 | -2.531650 | -1.337250 |
| 0.5 | 0.1 | 1.0 | | | | | | -0.650896 | -1.414150 | -1.216560 | -0.644890 | -1.415950 | -1.074150 |
| | 0.3 | | | | | | | -0.667759 | -1.409250 | -1.209530 | -0.662121 | -1.410750 | -1.063360 |
| | 0.5 | | | | | | | -0.691586 | -1.405320 | -1.131580 | -0.687573 | -1.405850 | -1.054350 |
| 0 | 0.5 | | | | | | | -1.056580 | -0.278257 | -0.092785 | -1.485415 | -0.27852 | -0.094245 |
| 0.5 | | | | | | | | -1.294280 | -0.274000 | -0.093990 | -1.496452 | -0.27857 | -0.093652 |
| 1 | | | | | | | | -1.49736 | -0.270456 | -0.095407 | -1.552457 | -0.27292 | -0.092245 |

## 5. Conclusions

The present paper studies the effect of chemical reaction on mixed convective steady two-dimensional boundary layer flow of an incompressible non-Newtonian (Casson) fluid over a vertical stretching sheet with variable viscosity, variable thermal conductivity, and variable diffusivity in a porous medium. The main conclusions from the analysis of the obtained results using OHAM are:

(i) The velocity profile is enhanced for increasing values of mixed convection parameters and the opposite is observed for variable viscosity, velocity exponent, and permeability parameters.

(ii) The temperature profile increases for increasing values of the variable viscosity and thermal conductivity, permeability, and radiation parameters. The opposite effect occurs in the case of mixed convection parameters, velocity exponent parameters, and Prandtl number.

(iii) The chemical species concentration increases as the variable viscosity parameter, variable species diffusivity parameter permeability parameter increases and the reverse effect occurs for mixed convection parameters, velocity exponent parameter, Schmidt number, and reaction rate parameter.

## Acknowledgment

One of the authors (Neelufer Z Basha) is thankful to the Vijayanagara Sri Krishnadevaraya University, Ballari for the financial support under the "Seed Money Project Grant for Young Faculty" scheme.

## References

[1] Liao, Shijun. *Homotopy analysis method in nonlinear differential equations*. Beijing: Higher Education Press, 2012. https://doi.org/10.1007/978-3-642-25132-0

[2] Krishna, M. Veera, and Ali J. Chamkha. "Hall and ion slip effects on MHD rotating boundary layer flow of nanofluid past an infinite vertical plate embedded in a porous medium." *Results in Physics* 15 (2019): 102652. https://doi.org/10.1016/j.rinp.2019.102652

[3] Krishna, M. Veera, and Ali J. Chamkha. "Hall and ion slip effects on magnetohydrodynamic convective rotating flow of Jeffreys fluid over an impulsively moving vertical plate embedded in a saturated porous medium with Ramped wall temperature." *Numerical Methods for Partial Differential Equations* 37, no. 3 (2021): 2150-2177. https://doi.org/10.1002/num.22670

[4] Krishna, M. Veera. "Hall and ion slip impacts on unsteady MHD free convective rotating flow of Jeffreys fluid with ramped wall temperature." *International Communications in Heat and Mass Transfer* 119 (2020): 104927. https://doi.org/10.1016/j.icheatmasstransfer.2020.104927

[5] Krishna, M. Veera, B. V. Swarnalathamma, and Ali J. Chamkha. "Investigations of Soret, Joule and Hall effects on MHD rotating mixed convective flow past an infinite vertical porous plate." *Journal of Ocean Engineering and Science* 4, no. 3 (2019): 263-275. https://doi.org/10.1016/j.joes.2019.05.002

[6] Krishna, M. Veera, N. Ameer Ahamad, and Ali J. Chamkha. "Hall and ion slip effects on unsteady MHD free convective rotating flow through a saturated porous medium over an exponential accelerated plate." *Alexandria Engineering Journal* 59, no. 2 (2020): 565-577. https://doi.org/10.1016/j.aej.2020.01.043

[7] Krishna, M. Veera, Kamboji Jyothi, and Ali J. Chamkha. "Heat and mass transfer on unsteady, magnetohydrodynamic, oscillatory flow of second-grade fluid through a porous medium between two vertical plates, under the influence of fluctuating heat source/sink, and chemical reaction." *International Journal of Fluid Mechanics Research* 45, no. 5 (2018). https://doi.org/10.1615/InterJFluidMechRes.2018024591

[8] Krishna, M. Veera. "Hall and ion slip effects on radiative MHD rotating flow of Jeffreys fluid past an infinite vertical flat porous surface with ramped wall velocity and temperature." *International Communications in Heat and Mass Transfer* 126 (2021): 105399. https://doi.org/10.1016/j.icheatmasstransfer.2021.105399

[9] Krishna, M. Veera, and Ali J. Chamkha. "Hall and ion slip effects on MHD rotating flow of elastico-viscous fluid through porous medium." *International Communications in Heat and Mass Transfer* 113 (2020): 104494. https://doi.org/10.1016/j.icheatmasstransfer.2020.104494

[10] Krishna, M. Veera, Kamboji Jyothi, and Ali J. Chamkha. "Heat and mass transfer on MHD flow of second-grade fluid through porous medium over a semi-infinite vertical stretching sheet." *Journal of Porous Media* 23, no. 8 (2020). https://doi.org/10.1615/JPorMedia.2020023817

[11] Abbas, Amir, Muhammad Ashraf, Hafeez Ahmad, Kaouther Ghachem, Zia Ullah, Abid Hussanan, Taher Labidi, and Lioua Kolsi. "Computational analysis of Darcy-Forchheimer relation, reduced gravity, and external applied magnetic field influence on radiative fluid flow and heat transfer past a sphere: Finite difference method." *Heliyon* 9, no. 5 (2023). https://doi.org/10.1016/j.heliyon.2023.e15696

[12] Abbas, Amir, Muhammad Ashraf, Ioannis E. Sarris, Kaouther Ghachem, Taher Labidi, Lioua Kolsi, and Hafeez Ahmad. "Numerical Simulation of the Effects of Reduced Gravity, Radiation and Magnetic Field on Heat Transfer Past a Solid Sphere Using Finite Difference Method." *Symmetry* 15, no. 3 (2023): 772. https://doi.org/10.3390/sym15030772

[13] Abbas, Amir, Asma Noreen, Masood Ashraf Ali, Muhammad Ashraf, Eman Alzahrani, Riadh Marzouki, and M. Goodarzi. "Solar radiation over a roof in the presence of temperature-dependent thermal conductivity of a Casson flow for energy saving in buildings." *Sustainable Energy Technologies and Assessments* 53 (2022): 102606. https://doi.org/10.1016/j.seta.2022.102606

[14] Abbas, Amir, Ioannis E. Sarris, Muhammad Ashraf, Kaouther Ghachem, Nidhal Hnaien, and Badr M. Alshammari. "The Effects of Reduced Gravity and Radiative Heat Transfer on the Magnetohydrodynamic Flow Past a Non-Rotating Stationary Sphere Surrounded by a Porous Medium." *Symmetry* 15, no. 4 (2023): 806. https://doi.org/10.3390/sym15040806

[15] Ewis, Karem Mahmoud. "Effects of Variable Thermal Conductivity and Grashof Number on Non-Darcian Natural Convection Flow of Viscoelastic Fluids with Non Linear Radiation and Dissipations." *Journal of Advanced Research in Applied Sciences and Engineering Technology* 22, no. 1 (2021): 69-80. https://doi.org/10.37934/araset.22.1.6980

[16] Jahan, Sultana, M. Ferdows, M. D. Shamshuddin, and Khairy Zaimi. "Effects of solar radiation and viscous dissipation on mixed convective non-isothermal hybrid nanofluid over moving thin needle." *Journal of Advanced Research in Micro and Nano Engineering* 3, no. 1 (2021): 1-11.

[17] Akaje, Wasiu, and B. I. Olajuwon. "Impacts of Nonlinear thermal radiation on a stagnation point of an aligned MHD Casson nanofluid flow with Thompson and Troian slip boundary condition." *Journal of Advanced Research in Experimental Fluid Mechanics and Heat Transfer* 6, no. 1 (2021): 1-15.

[18] Chambré, Paul L., and Jonathan D. Young. "On the diffusion of a chemically reactive species in a laminar boundary layer flow." *The Physics of Fluids* 1, no. 1 (1958): 48-54. https://doi.org/10.1063/1.1724336

[19] Muthucumaraswamy, R. "Effects of a chemical reaction on a moving isothermal vertical surface with suction." *Acta Mechanica* 155, no. 1-2 (2002): 65-70. https://doi.org/10.1007/BF01170840

[20] Chamkha, Ali J. "MHD flow of a uniformly stretched vertical permeable surface in the presence of heat generation/absorption and a chemical reaction." *International Communications in Heat and Mass Transfer* 30, no. 3 (2003): 413-422. https://doi.org/10.1016/S0735-1933(03)00059-9

[21] Sohail, Ayesha, M. J. Uddin, and M. M. Rashidi. "Numerical study of free convective flow of a nanofluid over a chemically reactive porous flat vertical plate with a second-order slip model." *Journal of Aerospace Engineering* 29, no. 2 (2016): 04015047. https://doi.org/10.1061/(ASCE)AS.1943-5525.0000544

[22] Basha, N. Z., C. Rajashekhar, F. Mebarek-Oudina, K. V. Prasad, H. Vaidya, Kamel Guedri, Attia Boudjemline, Rami Mansouri, and Ahmed Taieb. "Sutterby hybrid nanofluid flow and heat transfer over a nonlinearly expanding sheet with convective boundary condition and zero-mass flux concentration." *International Journal of Modern Physics B* (2023): 2450146. https://doi.org/10.1142/S0217979224501467

[23] Ashraf, Muhammad, Anwar Khan, Amir Abbas, Abid Hussanan, Kaouther Ghachem, Chemseddine Maatki, and Lioua Kolsi. "Finite Difference Method to Evaluate the Characteristics of Optically Dense Gray Nanofluid Heat Transfer around the Surface of a Sphere and in the Plume Region." *Mathematics* 11, no. 4 (2023): 908. https://doi.org/10.3390/math11040908

[24] Abbas, Amir, Abderrahim Wakif, Maria Shafique, Hafeez Ahmad, Qurat ul ain, and Taseer Muhammad. "Thermal and mass aspects of Maxwell fluid flows over a moving inclined surface via generalized Fourier's and Fick's laws." *Waves in Random and Complex Media* (2023): 1-27. https://doi.org/10.1080/17455030.2023.2198612

[25] Abbas, Amir, Radhika Khandelwal, Hafeez Ahmad, Asifa Ilyas, Liaqat Ali, Kaouther Ghachem, Walid Hassen, and Lioua Kolsi. "Magnetohydrodynamic Bioconvective Flow of Williamson Nanofluid over a Moving Inclined Plate Embedded in a Porous Medium." *Mathematics* 11, no. 4 (2023): 1043. https://doi.org/10.3390/math11041043

[26] Rosali, Haliza, Mohd Noor Badlilshah, Mohamat Aidil Mohamat Johari, and Norfifah Bachok. "Unsteady boundary layer stagnation point flow and heat transfer over a stretching sheet in a porous medium with slip effects." *CFD Letters* 12, no. 10 (2020): 52-61. https://doi.org/10.37934/cfdl.12.10.5261

[27] Abubakar, Saidu Bello, Nor Azwadi Che Sidik, and Siti Nurul Akmal Yusof. "Measurement of Fluid Flow and Heat Transfer Performance in Rectangular Microchannel using Pure Water and $Fe_3O_4$-$H_2O$ Nanofluid." *Journal of Advanced Research in Applied Mechanics* 68, no. 1 (2020): 9-21. https://doi.org/10.37934/aram.68.1.921

[28] Ewis, Karem Mahmoud. "Analytical solution of modified Bingham fluid flow through parallel plates channel subjected to forchheimer medium and Hall current using linearized differential transformation method." *Journal of Advanced Research in Numerical Heat Transfer* 4, no. 1 (2021): 14-31.
[29] Vajravelu, K., K. V. Prasad, and Hanumesh Vaidya. "Influence of Hall Current on MHD Flow and Heat Transfer over a slender stretching sheet in the presence of variable fluid properties." *Communications in Numerical Analysis* 1, no. 2016 (2016): 17-36. https://doi.org/10.5899/2016/cna-00251
[30] Prasad, K. V., Hanumesh Vaidya, and K. Vajravelu. "MHD mixed convection heat transfer over a non-linear slender elastic sheet with variable fluid properties." Applied Mathematics and Nonlinear Sciences 2, no. 2 (2017): 351-366. https://doi.org/10.21042/AMNS.2017.2.00000
[31] Prasad, K. V., K. Vajravelu, Hanumesh Vaidya, and Robert A. Van Gorder. "MHD flow and heat transfer in a nanofluid over a slender elastic sheet with variable thickness." *Results in Physics* 7 (2017): 1462-1474. https://doi.org/10.1016/j.rinp.2017.03.022
[32] Abbasi, A., Sami Ullah Khan, Kamel Al-Khaled, M. Ijaz Khan, W. Farooq, Ahmed M. Galal, Khurram Javid, and M. Y. Malik. "Thermal prospective of Casson nano-materials in radiative binary reactive flow near oblique stagnation point flow with activation energy applications." *Chemical Physics Letters* 786 (2022): 139172. https://doi.org/10.1016/j.cplett.2021.139172
[33] Raza, Ali, Sami Ullah Khan, Kamel Al-Khaled, M. Ijaz Khan, Absar Ul Haq, Fakhirah Alotaibi, A. Mousa Abd Allah, and Sumaira Qayyum. "A fractional model for the kerosene oil and water-based Casson nanofluid with inclined magnetic force." *Chemical Physics Letters* 787 (2022): 139277. https://doi.org/10.1016/j.cplett.2021.139277
[34] Li, Yun-Xiang, M. Israr Ur Rehman, Wen-Hua Huang, M. Ijaz Khan, Sami Ullah Khan, Ronnason Chinram, and S. Kadry. "Dynamics of Casson nanoparticles with non-uniform heat source/sink: A numerical analysis." *Ain Shams Engineering Journal* 13, no. 1 (2022): 101496. https://doi.org/10.1016/j.asej.2021.05.010
[35] Al-Khaled, Kamel, and Sami Ullah Khan. "Thermal aspects of casson nanoliquid with gyrotactic microorganisms, temperature-dependent viscosity, and variable thermal conductivity: Bio-technology and thermal applications." *Inventions* 5, no. 3 (2020): 39. https://doi.org/10.3390/inventions5030039
[36] Prasad, K. V., K. Vajravelu, Hanumesh Vaidya, Neelufer Z. Basha, and V. Umesh. "Thermal and species concentration of MHD Casson fluid at a vertical sheet in the presence variable fluid properties." *Ain Shams Engineering Journal* 9, no. 4 (2018): 1763-1779. https://doi.org/10.1016/j.asej.2016.08.017
[37] Prasad, K. V., K. Vajravelu, I. S. Shivakumara, Hanumesh Vaidya, and Neelufer Basha. "Flow and heat transfer of a Casson Nanofluid over a nonlinear stretching sheet." *Journal of Nanofluids* 5, no. 5 (2016): 743-752. https://doi.org/10.1166/jon.2016.1255
[38] Fan, Tao, and Xiangcheng You. "Optimal homotopy analysis method for nonlinear differential equations in the boundary layer." *Numerical Algorithms* 62 (2013): 337-354. https://doi.org/10.1007/s11075-012-9587-5
[39] Vajravelu, K., K. V. Prasad, and Chiu-On Ng. "Unsteady convective boundary layer flow of a viscous fluid at a vertical surface with variable fluid properties." *Nonlinear Analysis: Real World Applications* 14, no. 1 (2013): 455-464. https://doi.org/10.1016/j.nonrwa.2012.07.008
[40] Ishak, Anuar, Roslinda Nazar, and Ioan Pop. "Boundary layer flow and heat transfer over an unsteady stretching vertical surface." *Meccanica* 44 (2009): 369-375. https://doi.org/10.1007/s11012-008-9176-9
[41] Ali, Mohamed E. "Heat transfer characteristics of a continuous stretching surface." *Wärme-und Stoffübertragung* 29, no. 4 (1994): 227-234. https://doi.org/10.1007/BF01539754